Nanoscale Advances

ROYAL SOCIETY OF CHEMISTRY

PAPER

View Article Online
View Journal | View Issue

Cite this: *Nanoscale Adv.*, 2025, **7**, 8104

From botanical waste to a biocatalyst: *Kigelia pinnata* flower-derived CQDs for triazolidine-3-thione synthesis and their *in silico* evaluation

Sunita Teli, [a] Shivani Soni, [a] Nisarg Rana,[b] Anu Manhas [b] and Shikha Agarwal *[a]

Biowaste-derived carbon quantum dots (CQDs) have emerged as sustainable, low-cost nanomaterials that align with the principles of green chemistry and promote waste-to-wealth conversion. In this work, CQDs were synthesized using drop-down flowers of *Kigelia pinnata* as a novel biowaste carbon source *via* a green hydrothermal method. The resulting CQDs were comprehensively characterized by HRTEM, FT-IR, UV-visible, fluorescence spectroscopy, EDS, and XRD, revealing well-dispersed spherical particles with an average diameter of 3.78 nm. They showed excellent catalytic activity as an efficient nanocatalyst for the green synthesis of 1,2,4-triazolidine-3-thione derivatives using ethanol : water (1 : 4) mixture at RT, affording excellent yields (82–97%) in short reaction times (5–20 min). Three of the nine synthesized compounds are new, and the catalyst was reusable for up to six runs without significant loss of activity. The protocol offers key advantages, *viz.,* broad substrate scope, mild conditions, gram-scale feasibility, and favorable green chemistry metrics. Furthermore, all the synthesized compounds were screened for biological activity using PASS prediction, followed by molecular docking with 17β-dehydrogenase (4DBW) and pterin deaminase (3H23). The docking studies showed stable interactions and favorable binding energies, suggesting good affinity for both enzymes. The compounds also exhibited promising drug-like behavior based on ADMET analysis.

Received 1st August 2025
Accepted 31st October 2025

DOI: 10.1039/d5na00734h

rsc.li/nanoscale-advances

1 Introduction

In recent years, nanotechnology has emerged as a transformative field with broad applications across materials science, medicine, energy, and environmental remediation.[1,2] This revolution is mainly driven by nanomaterials, whose unique physicochemical properties at the nanoscale make them highly adaptable for diverse applications. Among the various classes of nanomaterials, carbon-based nanostructures have attracted immense attention due to their remarkable versatility, high surface area, high strength, biocompatibility, good electron conductivity, and eco-friendly nature.[3,4] These include graphene, carbon nanotubes, fullerenes, and, more recently, carbon quantum dots (CQDs), a new generation class of carbon-based nanomaterials that combine the electronic properties of traditional quantum dots with the low toxicity and biocompatibility of carbon.[5]

CQDs are quasi-spherical nanoparticles, often smaller than 10 nm in size, exhibiting unique optical properties such as excitation-dependent fluorescence, chemical stability, and high water dispersibility.[6] Since their discovery, CQDs have been extensively explored for applications in bioimaging, sensing, drug delivery, photovoltaics, and as metal-free catalysts in organic synthesis.[7,8] Over the last decade, CQDs synthesized from renewable biomass sources have garnered considerable interest, aligning with the principles of green chemistry and sustainability. Utilizing agro-industrial or plant-derived waste not only addresses environmental concerns associated with waste disposal but also provides an economical and scalable route for nanomaterial production. In this context, the synthesis of CQDs from biogenic resources offers dual benefits: valorization of waste and the generation of functional carbon-based nanocatalysts. Various biowastes such as fruit peels, leaves, wood, flowers and plant extracts have been explored as carbon precursors.[8] As per an exhaustive literature survey, flowers of *Kigelia pinnata* have not been reported as a carbon source for CQD synthesis. The present study highlights the hydrothermal synthesis of CQDs using *Kigelia pinnata* flowers (KP-CQDs), presenting a novel and sustainable carbon precursor. The resulting KP-CQDs were thoroughly characterized and subsequently employed as a highly effective and eco-friendly nanocatalyst for the preparation of nitrogen-containing heterocyclic compounds.

Heterocyclic compounds, especially those containing N-atoms, represent an indispensable class of organic molecules

[a]*Synthetic Organic Chemistry Laboratory, Department of Chemistry, Mohanlal Sukhadia University, Udaipur-313001, Rajasthan, India. E-mail: shikhaagarwal@mlsu.ac.in*

[b]*Department of Chemistry, School of Energy Technology, Pandit Deendayal Energy University, Gandhinagar, 382426, India*

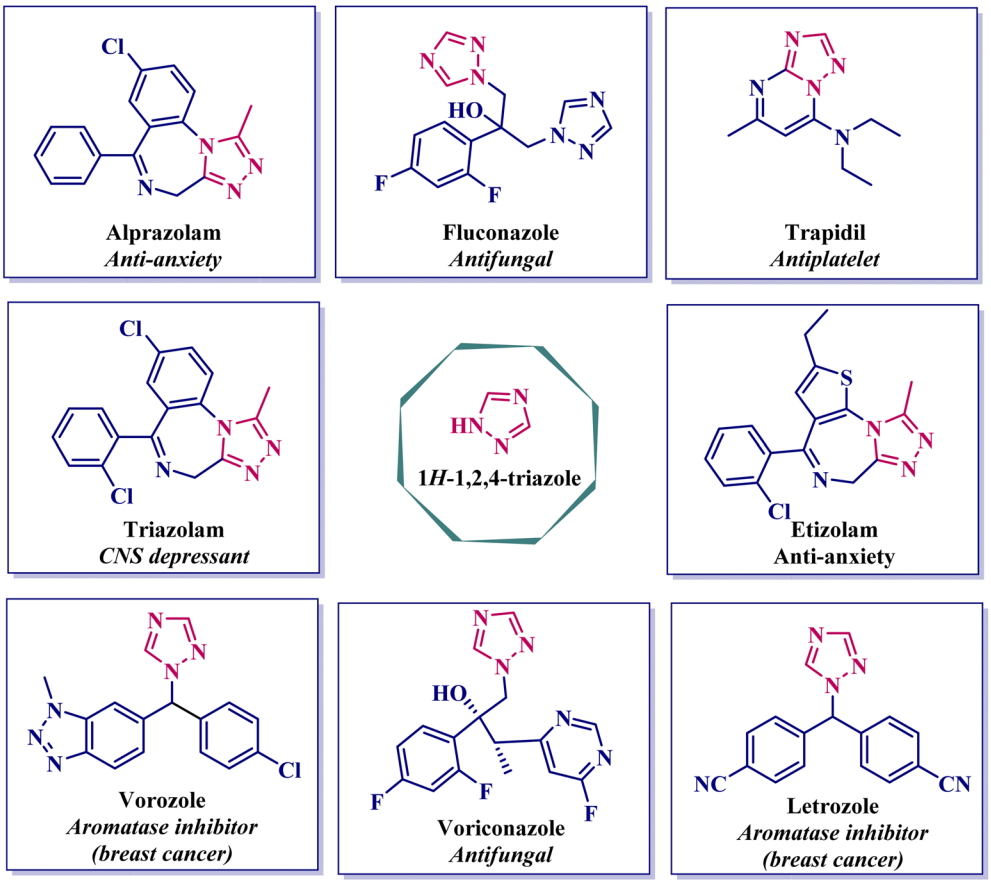

Fig. 1 Some pharmacologically active molecules containing 1,2,4-triazole moieties.[24,25]

due to their prevalence in natural products, pharmaceuticals, agrochemicals, and advanced materials.[9,10] Among these, 1,2,4-triazolidine derivatives have received growing interest for their broad spectrum of biological activities, such as antimicrobial,[11–13] anticancer,[14] anti-inflammatory, antitubercular,[13] antioxidant,[12] antifungal,[15] antiviral,[16] acetylcholinesterase inhibition,[17,18] anti-HIV,[19] antidepressant,[20] anti-allergic,[21] antiepileptic,[22] and analgesic[23] properties. Fig. 1 highlights various pharmacologically relevant molecules incorporating the 1,2,4-triazole scaffold.[24,25] These compounds often serve as important pharmacophores in medicinal chemistry and as intermediates in drug development. Traditionally, the synthesis of triazolidines relied on acid catalysts such as sulfamic acid,[26] $[(Py)_2SO][HSO_4]_2$,[27] [2-HMPyBSA]HSO_4,[28] glycine nitrate,[29] PEG-400,[30] acetic acid[31] *etc.* More recently, greener alternatives have been explored, including ionic liquids,[32] magnetic nanocatalysts,[33,34] agro-waste-derived catalysts[24] and organocatalysts.[25,35,36] However, these approaches may still involve non-renewable materials or complex catalyst preparation steps. They often involve high temperatures, long reaction durations, metal involvement, limited substrate versatility or the need for microwave (MW) irradiation. For example, the synthesis involving magnetic nanoparticles demanded the use of a chemical reducing agent ($NaBH_4$) and required heating under reflux conditions for more than half an hour.[37] In contrast, the approach utilizing orange peel ash water extract relied on MW-assisted irradiation at 130 °C.[24] Therefore, the development of more sustainable, greener, and efficient synthetic protocols for triazolidines remains a critical goal.

In the present work, we have demonstrated a facile and green approach for the formation of triazolidine derivatives using KP-CQDs as a metal-free, biowaste-derived nanocatalyst for the first time. A total of 9 compounds were synthesized, including 3 new triazolidine-3-thiones (T-3-Ts) *via* reaction of carbonyl compounds with thiosemicarbazide (TSC). Moreover, the derivatives were also evaluated for their pharmacological potential through molecular docking. Based on PASS analysis,[38] two biologically relevant targets were selected: Pterin deaminase (PDB ID: 3H23)[39] and testosterone 17β-dehydrogenase ($NADP^+$) (PDB ID: 4DBW).[39] Notably, this is the first report exploring the docking potential of 1,2,4-triazolidines against these two targets, offering new insights into their prospective pharmacological applications. Furthermore, these molecules were studied under ADMET studies to predict their pharmacokinetic properties.

2 Results and discussion

2.1. Study of KP-CQDs

For this research, drop-down flowers of *Kigelia pinnata* were utilized as a novel carbon source for synthesizing KP-CQDs through the hydrothermal method. The resulting CQDs were

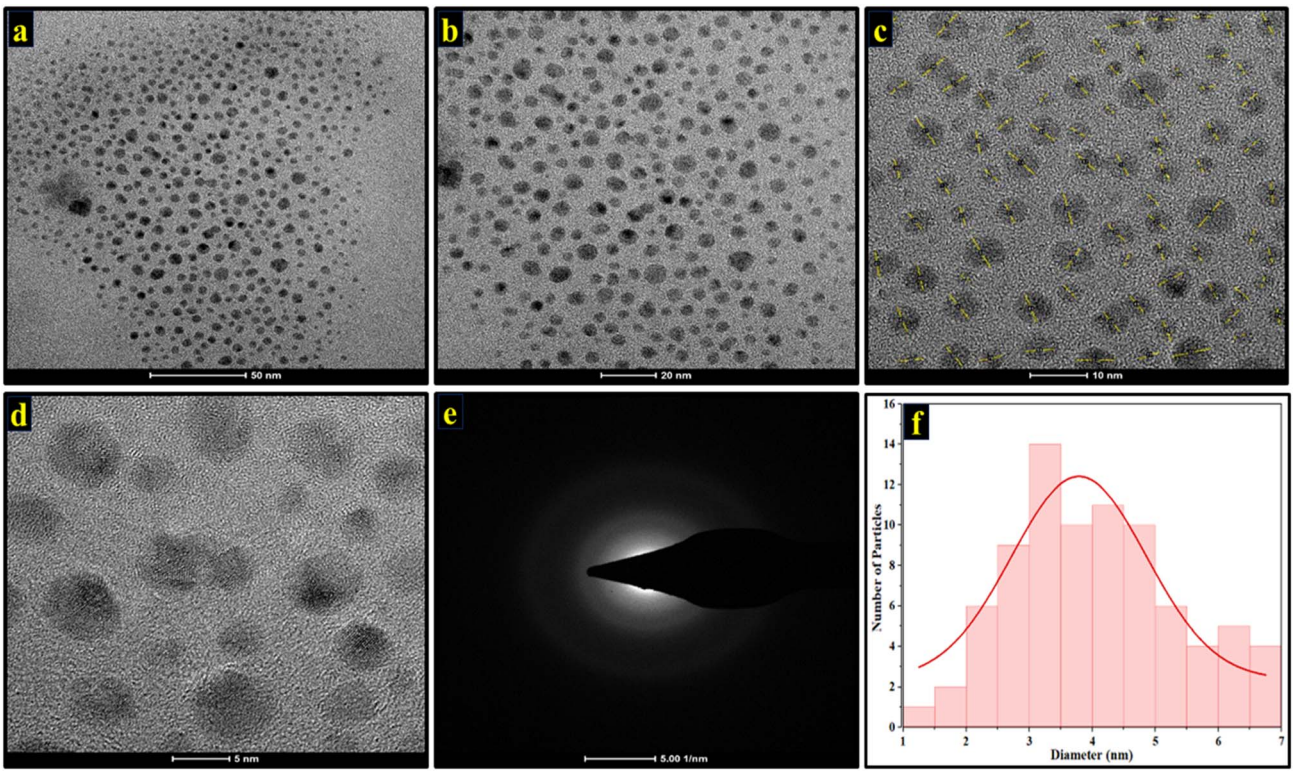

Fig. 2 HRTEM images of KP-CQDs at varying resolutions: (a) 50 nm, (b) 20 nm, (c) 10 nm, and (d) 5 nm; (e) SAED pattern; (f) size distribution histogram of KP-CQDs at 10 nm resolution.

thoroughly examined using various techniques, including HRTEM, EDS, FT-IR, XRD, UV-Visible, and fluorescence spectroscopy. HRTEM (300 kV) was employed to verify the successful formation of KP-CQDs and to examine their morphology and particle size. Fig. 2a–d present HRTEM images at different magnifications, clearly revealing that the KP-CQDs are uniformly distributed and possess a spherical shape.[40,41] The SAED pattern further confirms the amorphous nature of the synthesized dots (Fig. 2e).[42] The particle size distribution histogram (Fig. 2f) demonstrates an average diameter of 3.78 nm, which confirms the successful synthesis of KP-CQDs. The average particle size was calculated using ImageJ-win64 (Fiji) and OriginPro 2024b software.

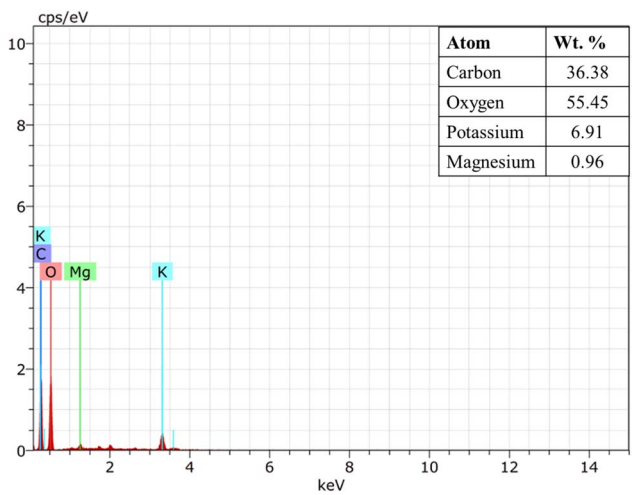

Atom	Wt. %
Carbon	36.38
Oxygen	55.45
Potassium	6.91
Magnesium	0.96

Fig. 3 EDX spectrum of KP-CQDs.

EDX was performed to determine the elemental composition of the synthesized KP-CQDs. The results, as shown in Fig. 3, indicate that the KP-CQDs consist of carbon (36.38%) and oxygen (55.45%).[43] These findings confirm that carbon and oxygen are the dominant elements present in the KP-CQD framework. The presence of K and Mg might be due to their natural abundance in biomass.

The FT-IR spectrum (Fig. 4) displays a strong, broad absorption band at 3316 cm^{-1}, which corresponds to the stretching vibration mode of the O–H bond.[44] A sharp peak observed at 1636 cm^{-1} is attributed to the stretching vibrations of the C=O bond (carboxylic), while the band at 624 cm^{-1} is associated with O–H bending vibrations.[41,43,45] These FT-IR spectral features indicate the presence of hydrophilic functional groups such as –OH & –COOH on the surface of the KP-CQDs.

As illustrated in Fig. 5, XRD analysis was carried out to analyze the crystallographic nature of KP-CQDs. The pattern displays two broad diffraction peaks at $2\theta = 29.5°$ and at $2\theta = 42.3°$, which correspond to the lattice planes (002) and (001), respectively.[46,47] The broad nature of the (002) peak suggests a low degree of graphitization, which is characteristic of an amorphous carbon nature typically formed during the hydrothermal process.[48,49]

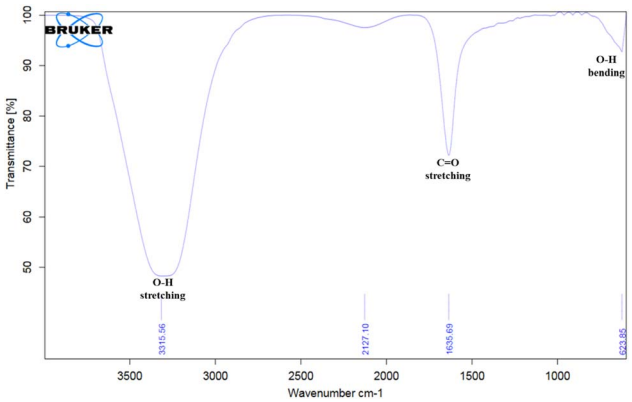

Fig. 4 FT-IR spectrum of KP-CQDs.

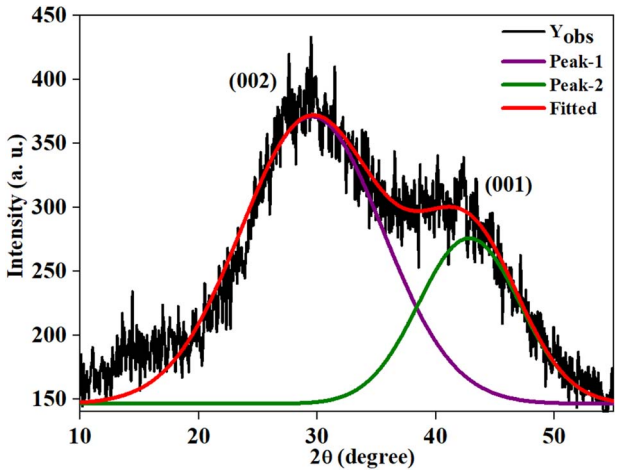

Fig. 5 XRD pattern of KP-CQDs.

The average crystallite size (D) of the synthesized KP-CQDs can be determined using the Debye–Scherrer equation[50] as follows:

$$D = \frac{0.9\lambda}{\beta \cos \theta}$$

where λ represents the wavelength of the Cu-K_α source (λ = 1.5406 Å), θ is the Bragg angle and β denotes the full width at half maximum (FWHM) of the diffraction peak. The calculated value of D for KP-CQDs was found to be 0.71 nm. Furthermore, the average particle size determined from the Gaussian fit of the HRTEM histogram (Fig. 2e) was 3.78 nm, which is higher than the crystallite size. This difference arises because the grain or particle size is generally larger than the crystalline size.

Fig. 6 illustrates the optical properties of the synthesized KP-CQDs. Under UV light, they exhibit strong green fluorescence, highlighting their excellent photoluminescent behavior. The UV-visible absorption spectrum (Fig. 6a) shows a prominent band at 280 nm, which can be attributed to the n–π* transitions of C=O bonds and π–π* transitions of C=C bonds, indicating the presence of conjugated and oxygen-containing functional groups.[51,52] The fluorescence spectrum (Fig. 6b) reveals that the KP-CQDs exhibit excitation at 310 nm (broad emission range = 310 to 650 nm), with a strong emission peak at 435 nm, identifying it as the optimal emission wavelength.[53]

2.2. Catalytic activity

To evaluate the catalytic efficiency of KP-CQDs, a model reaction between 4-nitrobenzaldehyde (1 mmol) and TSC (1 mmol) was carried out under varied reaction parameters, and the findings are compiled in Table 1. Without a catalyst, the reaction proceeded in an EtOH–water (1 : 1) system at RT, and it afforded only 49% yield in 120 min (entry 1). However, when KP-CQDs (0.50 mL) were used as the catalyst under solvent-free conditions, the yield improved to 68% within 60 min (entry 2), which confirmed the catalytic potential of the synthesized catalyst. When different solvents (ethanol, water, and ethanol–water mixture) were tested, water as a solvent significantly enhanced the yield to 83% in just 15 min (entry 3), while ethanol provided 89% yield in 10 min (entry 4). Notably, ethanol and water combination as a solvent system in varying ratios (1 : 1, 1 : 2, 1 :

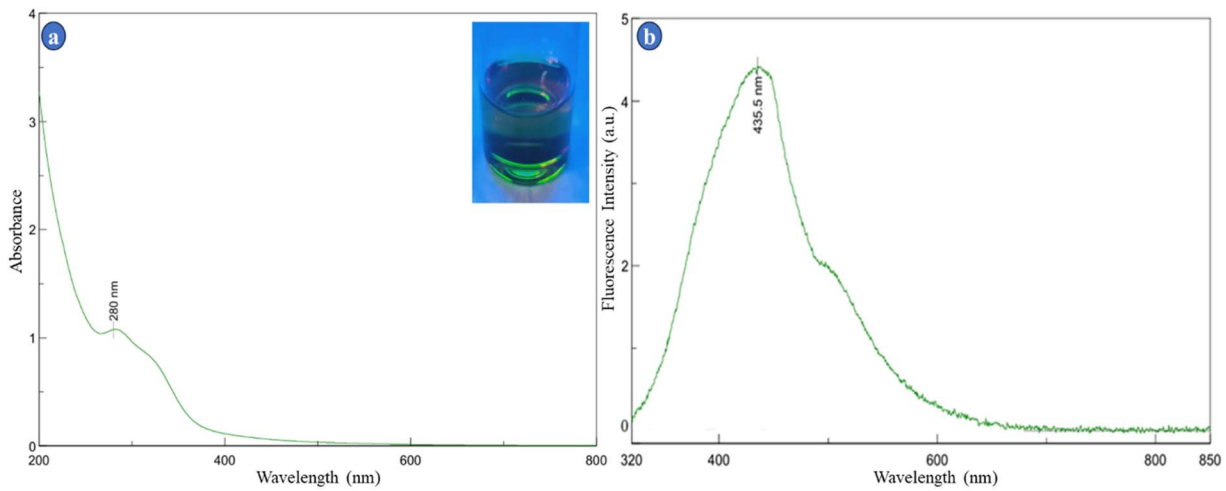

Fig. 6 UV-visible spectrum (a) and fluorescence emission spectrum (b) of KP-CQDs.

Table 1 Exploration of reaction variables for the preparation of 1,2,4-triazolidines[a,b,c]

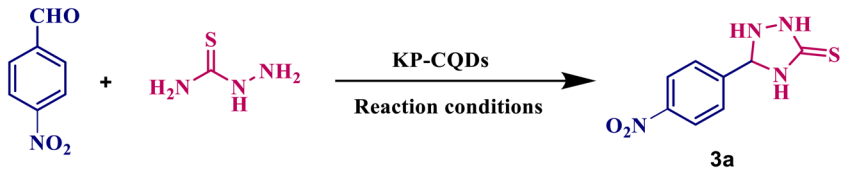

3a

S. No.	Catalyst (mL)	Solvent	Temperature	Time (min)	Yield (%)
1	—	EtOH + H_2O (1 : 1)	RT	120	49
2	KP-CQD (0.50)	Solvent-free	RT	60	68
3	KP-CQD (0.50)	Water	RT	15	83
4	KP-CQD (0.50)	Ethanol	RT	10	89
5	KP-CQD (0.50)	EtOH + H_2O (1 : 1)	RT	6	94
6	KP-CQD (0.50)	EtOH + H_2O (1 : 2)	RT	6	95
7	KP-CQD (0.50)	EtOH + H_2O (1 : 3)	RT	6	96
8	**KP-CQD (0.50)**	**EtOH + H_2O (1 : 4)**	**RT**	**6**	**97**
9	KP-CQD (0.25)	EtOH + H_2O (1 : 4)	RT	10	94
10	KP-CQD (1.00)	EtOH + H_2O (1 : 4)	RT	6	97
11	KP-CQD (0.50)	EtOH + H_2O (1 : 4)	80 °C	6	95
12[c]	KP-CQD (0.50)	EtOH + H_2O (1 : 4)	RT	10	92

[a] Reaction conditions: 4-nitrobenzaldehyde (1 mmol) + thiosemicarbazide (1 mmol), and the reaction completion was examined *via* TLC. [b] The most promising outcomes are marked in bold. [c] The reaction was performed using ultrasound assistance.

Table 2 Performance evaluation of various catalysts for 5-(4-nitrophenyl)-1,2,4-triazolidine-4-thione (**3a**) synthesis

S. No.	Catalyst (amount)	Reaction conditions	Time (min)	Yield (%)	Ref.
1	$C_5H_{10}[(2\text{-APy})_2(HSO_4)_2]$ (5 mol%)	EtOH + H_2O (4 : 6), RT	10	96	32
2	Water extract of orange fruit shell ash (3.5 mL)	M.W. (450 W), 130 °C	4	86	24
3	Fe_3O_4 magnetic nanoparticles (5 mol%)	$NaBH_4$ (eq. amount to reactants), EtOH, reflux	40	92	37
4	PEG-400 (0.5 mL)	80 °C	8	96	30
5	CuO nanoparticle (5 mg)	EtOH, 70 °C	6	94	54
6	**KP-CQDs (0.50 mL)**	**EtOH + H_2O (1 : 4), RT**	**6**	**97**	**This work**

3, or 1 : 4) further improved the reaction performance (entries 5–8). The ethanol–water (1 : 4) mixture was the most effective and delivered the highest yield of 97% in just 6 min at RT (entry 8). Reducing the catalyst volume to 0.25 mL slightly decreased the yield to 94% (entry 9), while increasing it to 1.00 mL maintained the highest yield (entry 10). Performing the reaction at a high temperature of 80 °C did not affect the yield (entry 11). Additionally, the reaction was also performed under ultrasonic conditions with KP-CQDs (0.50 mL) in an ethanol–water (1 : 4) system, and it gave 93% yield within 10 min (entry 12). These results highlight the high catalytic efficiency, rapid reaction rate, and environmentally friendly nature of KP-CQDs in the synthesis of triazolidines. Based on the optimization studies, the most effective reaction conditions were identified as using 0.50 mL of KP-CQDs at RT in an ethanol–water mixture (1 : 4), as shown in entry 8. These optimized parameters enabled the successful production of T-3-Ts moieties by reacting different aldehydes with TSC.

To further assess the catalytic performance of KP-CQDs, its efficiency was compared with previously reported methodologies, and the comparative findings are outlined in Table 2. While several catalysts, such as ionic liquids,[32] metal nanoparticles (Fe_3O_4 and CuO)[37,54] and biomass-based catalysts,[24] have shown high efficiency but they often involve limitations such as complex preparation, use of metal-based reagents, requirement for elevated temperatures or MW-assisted conditions. For instance, the use of Fe_3O_4 nanoparticles required a reducing agent ($NaBH_4$) and heating under reflux for 40 min,[37] while orange peel ash water extract required MW irradiation at 130 °C.[24] In our developed protocol, the reaction proceeded efficiently at RT in an EtOH–H_2O (1 : 4) system using KP-CQDs, delivering excellent yields without any metal, harsh conditions, or additives, highlighting the simplicity, eco-friendliness, and practicality of this approach. Moreover, their biological potential has also been unexplored. Building on this gap, the present work involved the CQD-catalyzed synthesis of these T-3-Ts scaffolds including 3 new compounds, along with their docking studies for pterin deaminase & 17β-dehydrogenase inhibition. Our approach not only aligns with green chemistry principles through the use of

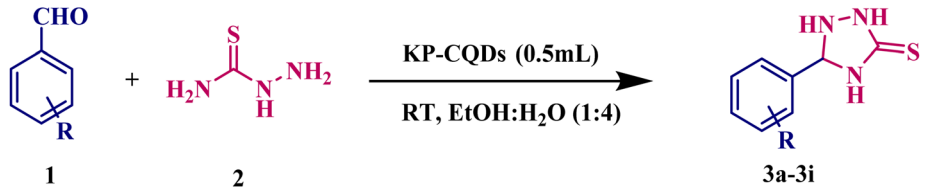

Scheme 1 General reaction for the T-3-Ts scaffolds.

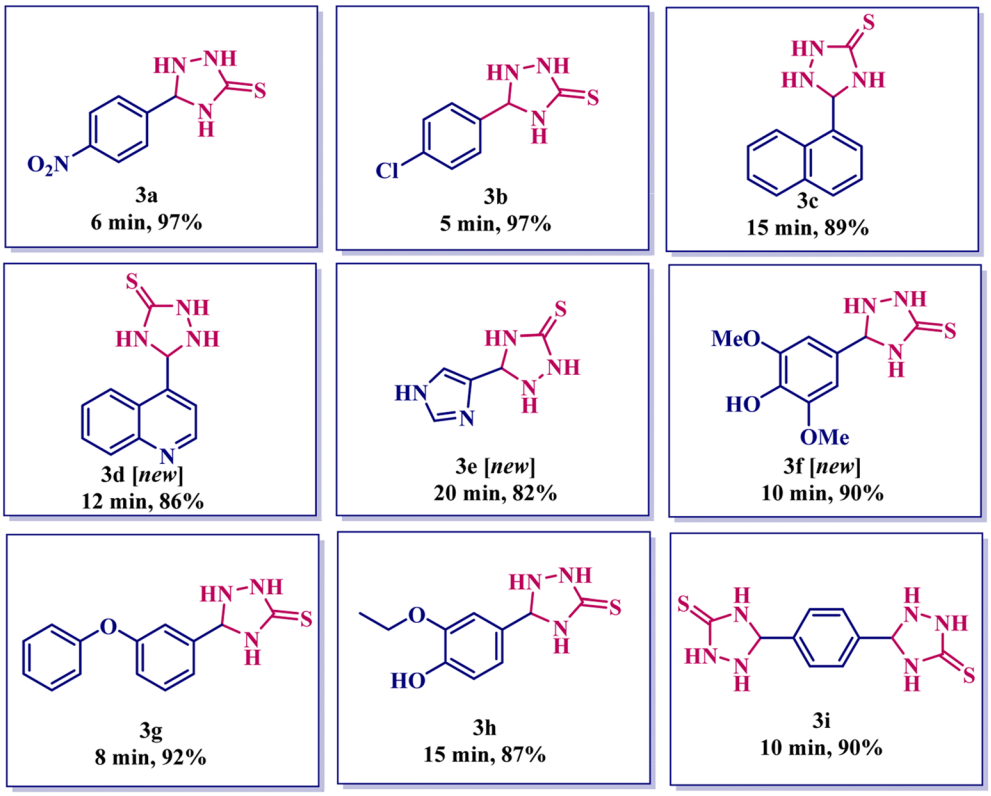

Scheme 2 Library of synthesized T-3-Ts scaffolds *via* KP-CQD catalysis (**3a–3i**).

a biogenic catalyst but also enriches the structural diversity of triazolidine derivatives, enhancing their dual significance across synthetic and pharmaceutical chemistry.

2.3. Synthesis of T-3-Ts

We have synthesized a library of 9 T-3-Ts derivatives *via* the reaction of various carbonyl compounds with TSC (Scheme 1). A wide range of aromatic aldehydes was employed to assess the substrate scope, which included electron-withdrawing groups (EWGs) such as 4-nitro, 4-chloro, and 3-phenoxy, and electron-donating groups (EDGs) such as 4-hydroxy-3,4-dimethoxy and 4-hydroxy-3-ethoxy. We also explored the reactivity of polycyclic aldehydes (1-naphthaldehyde) and heterocyclic aldehydes (quinoline-4-carbaldehyde and imidazole-4-carbaldehyde). To further explore multifunctional condensation, a dialdehyde (terephthalaldehyde) was employed to prepare bis-1,2,4-triazolidine derivative. As shown in Scheme 2, we have synthesized a total of 9 triazolidine scaffolds including 3 new compounds with remarkable yields (82–97%) in just 5–20 min. The structures of synthesized compounds were validated through ^{1}H & ^{13}C NMR spectroscopy and HRMS (Fig. S3–S22).

The proposed mechanism for the production of T-3-Ts scaffolds using KP-CQDs is depicted in Scheme 3, drawing insights from earlier reported methods.[25] Based on detailed characterization studies, it was confirmed that KP-CQDs possess hydroxyl and carboxyl functional groups, which play a crucial role in initiating the reaction. Initially, the catalyst protonated the carbonyl group of aldehydes (**1**) *via* hydrogen bonding, increasing its electrophilic character. This activation facilitated the nucleophilic attack by the amino group of TSC (**2**), which led to the formation of an intermediate (**b**). Subsequent elimination of a water molecule afforded the generation of an imine intermediate (**c**). In the final step, the second free amino group of TSC attacked the imine carbon, promoting intramolecular cyclization and yielding the desired product (**3**), while regenerating the catalyst.

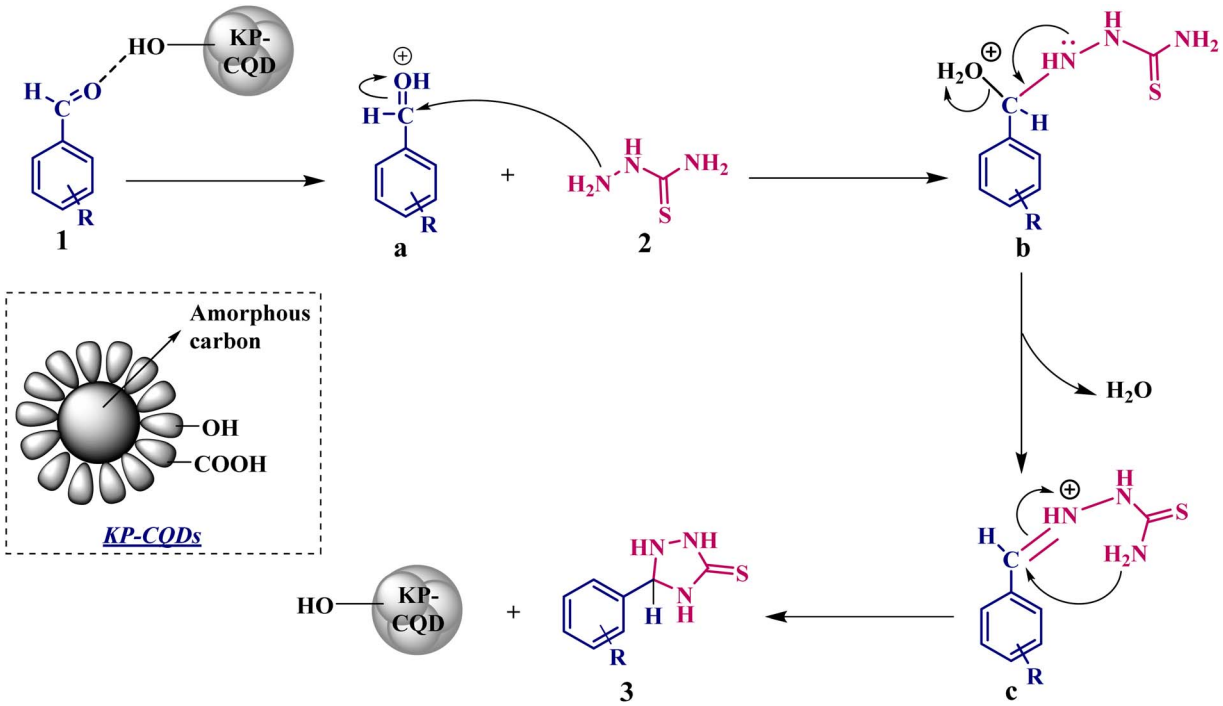

Scheme 3 Mechanistic pathway illustrating the KP-CQD-assisted formation of 1,2,4-triazolidines.

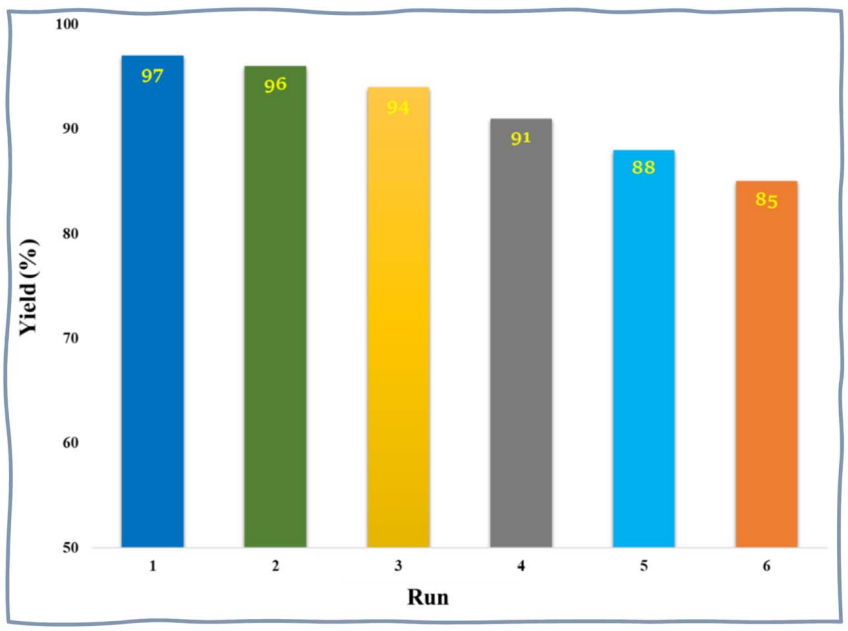

Fig. 7 Catalytic performance of KP-CQDs over six runs for the synthesis of compound **3b**.

2.4. Reusability

Upon completion of the reaction, the product and the catalyst were efficiently separated by simple filtration. The solid product was collected as a residue on the filter paper, while the filtrate—containing both the catalyst and the ethanol–water mixture—was collected and directly reused for subsequent reactions without any further purification. This process demonstrates the ease of catalyst recovery and reuse, requiring no additional steps such as solvent evaporation, washing, or drying. The KP-CQDs demonstrated excellent activity across several cycles, as illustrated in Fig. 7. The catalyst maintained a remarkable yield for up to four cycles, with only a slight decrease in yield from 95% to 91%. However, beyond the 4th cycle, a noticeable decline in catalytic efficiency was observed, with yields dropping to 88%

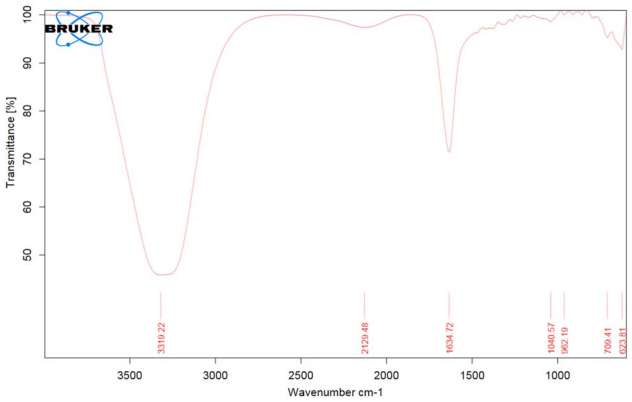

Fig. 8 FT-IR spectrum of reused KP-CQDs after six cycles.

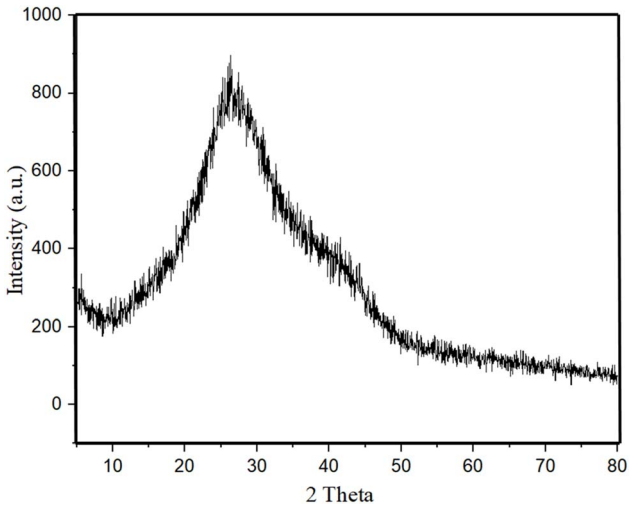

Fig. 9 XRD pattern of KP-CQDs after six catalytic cycles.

and 85% in the 5th and 6th cycles, respectively. A noticeable change in the catalyst's color was observed during repeated use, from dark brown to a lighter brown tone (Fig. S2a & S2b). Despite this visual change, the catalyst retained its characteristic green emission under UV light (Fig. S2c), suggesting its preserved optical and catalytic characters. To further assess the structural stability of the reused KP-CQDs, FT-IR (Fig. 8) and XRD (Fig. 9) analyses were performed, and the results were found to be identical to those of the freshly prepared KP-CQDs, confirming the preservation of their structural integrity after multiple catalytic cycles.

2.5. Gram scale reaction

To evaluate the potential for scale-up synthesis, the reaction was carried out under gram-scale conditions using the previously optimized protocol. For this, equimolar amounts of reactants: TSC (10 mmol, 0.911 g) and 4-chlorobenzaldehyde (10 mmol, 1.406 g) were reacted at RT in the presence of 0.50 mL of KP-CQDs and 30 mL of an ethanol : water (1 : 4) mixture as the solvent. The reaction was reached at completion within 10 min, as confirmed by TLC analysis. The product precipitated as a white solid out of the solution and readily separated from the catalyst and solvent *via* simple filtration. The residue was washed thoroughly with water to isolate the final product (**3b**). The product was obtained in excellent yield, 2.037 g or 95.63%, thereby demonstrating the scalability and efficiency of this green, catalyst-assisted method (Scheme 4 and Fig. S1).

2.6. Green chemistry metrics

Recent advances in synthetic chemistry have increasingly focused on the development of environmentally benign methodologies that align with the principles of green chemistry.[55,56] In this context, we utilized a biogenic KP-CQD catalyst to facilitate a sustainable and eco-conscious approach for the synthesis of 1,2,4-triazolidines. The proposed method demonstrated excellent green chemistry metrics, including high atom economy (88.62–93.78%), an impressive eco-score (80.78–88.44%), and efficient reaction mass performance (73.71–89.67%). Additionally, the process exhibited a favorable process mass intensity (1.129–1.378) and a low environmental factor (E-factor ≤0.357), highlighting the overall sustainability and minimal waste generation of the reaction system. Calculation of green metrics for all the synthesized compounds is detailed in the SI (Table S1).

2.7. Molecular docking

2.7.1. Activity prediction. To explore the potential biological activity of the synthesized 1,2,4-triazolidine derivatives, PASS online software[38] was used to predict the possible protein targets based on structural similarity and known bioactivity profiles. The predictions with probability of activity (Pa) > 0.5 were considered significant for the biological relevance (Table 3). Among the predicted targets, pterin deaminase and testosterone 17β-dehydrogenase ($NADP^+$) emerged as the most promising, with most of the synthesized compounds showing potential inhibitory activity against both enzymes. Pterin deaminase is an amidohydrolase enzyme that catalyzes the hydrolysis of pteridine compounds, forming lumazine

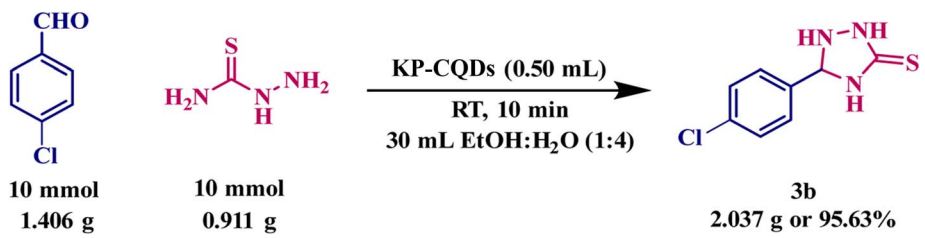

Scheme 4 Gram-scale production of 5-(4-chlorophenyl)-T-3-Ts (**3b**).

Table 3 The biological activities of compound '3i' were predicted using PASS online[a,b]

Pa	Pi	Activity
0.828	0.003	Chloride peroxidase inhibitor
0.727	**0.009**	**Pterin deaminase inhibitor**
0.747	**0.040**	**Testosterone 17beta-dehydrogenase (NADP$^+$) inhibitor**
0.732	0.025	Nicotinic alpha6beta3beta4alpha5 receptor antagonist
0.707	0.010	Thioredoxin inhibitor
0.733	0.053	Aspulvinone dimethylallyltransferase inhibitor
0.637	0.005	Albendazole monooxygenase inhibitor
0.655	0.026	Complement factor *D* inhibitor
0.701	0.076	Phobic disorders treatment

[a] Blue highlights indicate selected bioactivities with high predictive scores. [b] Compound with Pa > Pi is considered biologically active, and values of Pa > 0.5 indicate a high probability of activity.

derivatives and ammonia. This enzyme plays a crucial role in pterin metabolism and is indirectly involved in purine and pyrimidine pathways, which are essential for nucleic acid biosynthesis. Since its early discovery and patenting in 1959 for potential anticancer applications, pterin deaminase has gained increasing attention due to its implications in cell proliferation, immune modulation, and metabolic regulation.[57] Its inhibition has been linked to therapeutic effects in parasitic infections and inflammatory disorders, making it a valuable target for drug development. Testosterone 17β-dehydrogenase (NADP$^+$) is a key enzyme in steroid metabolism, particularly in the conversion of testosterone to androstenedione, and is associated with hormone-dependent diseases, including certain cancers and metabolic disorders. Inhibition of this enzyme has been explored for androgen-related therapeutic applications.

To investigate the binding affinity and interaction profiles of the synthesized molecules with these enzymes, molecular docking analysis was performed. Protein structures with PDB IDs 3H23 (for pterin deaminase) and 4DBW (for testosterone 17β-dehydrogenase NADP$^+$) were acquired from the RCSB Protein Data Bank. Importantly, as evidenced by existing reports, no previous *in silico* study has reported the evaluation of 1,2,4-triazolidines against these two biological targets, making this research a novel contribution to the area of triazolidine-based drug discovery.

2.7.2. ADMET studies. Over the last ten years, only a small number of drugs out of hundreds of candidates have been approved for the market because of the high failure rate during clinical trials. Two main causes of these failures are the lack of efficacy and unacceptable toxicity. Many potential therapeutic compounds failed in clinical trials due to poor ADMET properties. However, the experimental ADMET profiles are costly and time-consuming, so computational techniques that can predict ADMET have become an alternative approach. The ADMET studies were performed on all nine molecules (**3a–3i**) using AdmetSAR 3.0 to predict their pharmacokinetic and toxicity properties by studying parameters such as molecular weight (MW), total polar surface area (TPSA), permeability, and metabolism-related descriptors.[58] As shown in Table 4, all compounds followed Lipinski's rule of five, thus explaining their drug-likeness and oral bioavailability. The MW of the compounds ranged from 169.21 to 280.38 g mol^{-1}, which was well within the acceptable MW range. The TPSA values ranging from 36.09 Å to 79.23 Å also suggest an acceptable balance within polarity and permeability, thus indicating effective absorption. Moreover, Caco-2 permeability (−4.5 to −5.7) and human intestinal absorption (HIA) (>0.89) indicate that all the selected molecules possess the capability to be effectively absorbed in the gastrointestinal tract. A parameter such as blood–brain barrier (BBB), ranged within 0.62 to 0.97, displayed that compounds **3b**, **3c**, and **3g** possess the potential to cross the BBB, suggesting their CNS activity. Plasma protein binding (PPB) calculations ranging from 0.31 to 0.84 indicate moderate to high binding affinity. Hepatic metabolism (HLM) and renal clearance (CLr) values suggest the metabolic stability, whereas half-life (T50) suggests moderate elimination rate. Moreover, compounds remain within acceptable ranges for neurotoxicity and drug-induced liver injury (DILI) parameters. Overall, the ADMET analysis, when compared to the cut-off range in Table S2, almost all the molecules demonstrated acceptable results. Some of the molecules may be near the cut-off value for renal elimination (CLr), but they show better results in other parameters. Therefore, all the molecules show an acceptable range in most parameters and were selected for molecular docking.

2.7.3. Molecular docking studies

2.7.3.1 Redocking studies. Prior to docking, redocking was performed using B54 co-crystallised in the binding site of 3H23

Table 4 List of ADMET parameters generated for all the synthesized molecules[a]

Molecule	MW	TPSA	Caco_2	HIA	BBB	PPB	CYP2B6 inhibitor	HLM	CLr	T50	Neuro-toxicity	DILI
3a	224.245	79.23	−5.011	0.942	0.841	0.496	0.409	0.175	0.553	−0.461	−2.492	0.703
3b	213.693	36.09	−4.516	0.991	0.970	0.641	0.603	0.156	0.538	−1.054	−2.362	0.596
3c	229.308	36.09	−4.911	0.983	0.964	0.825	0.660	0.368	0.728	−0.708	−2.405	0.495
3d	230.296	48.98	−5.425	0.974	0.897	0.638	0.276	0.078	0.845	−0.479	−2.493	0.639
3e	169.213	64.77	−5.529	0.936	0.801	0.315	0.162	0.031	0.822	−0.273	−2.672	0.684
3f	255.299	74.78	−5.406	0.936	0.706	0.488	0.075	0.064	0.671	−0.546	−2.724	0.671
3g	271.345	45.32	−4.728	0.987	0.965	0.844	0.677	0.218	0.700	−0.863	−2.465	0.536
3h	239.3	65.55	−5.116	0.959	0.698	0.603	0.140	0.158	0.674	−0.376	−2.726	0.689
3i	280.382	72.18	−5.693	0.897	0.623	0.396	0.204	0.074	0.803	−0.282	−2.641	0.728

[a] Lipinski rule (**3a–3i**): accepted.

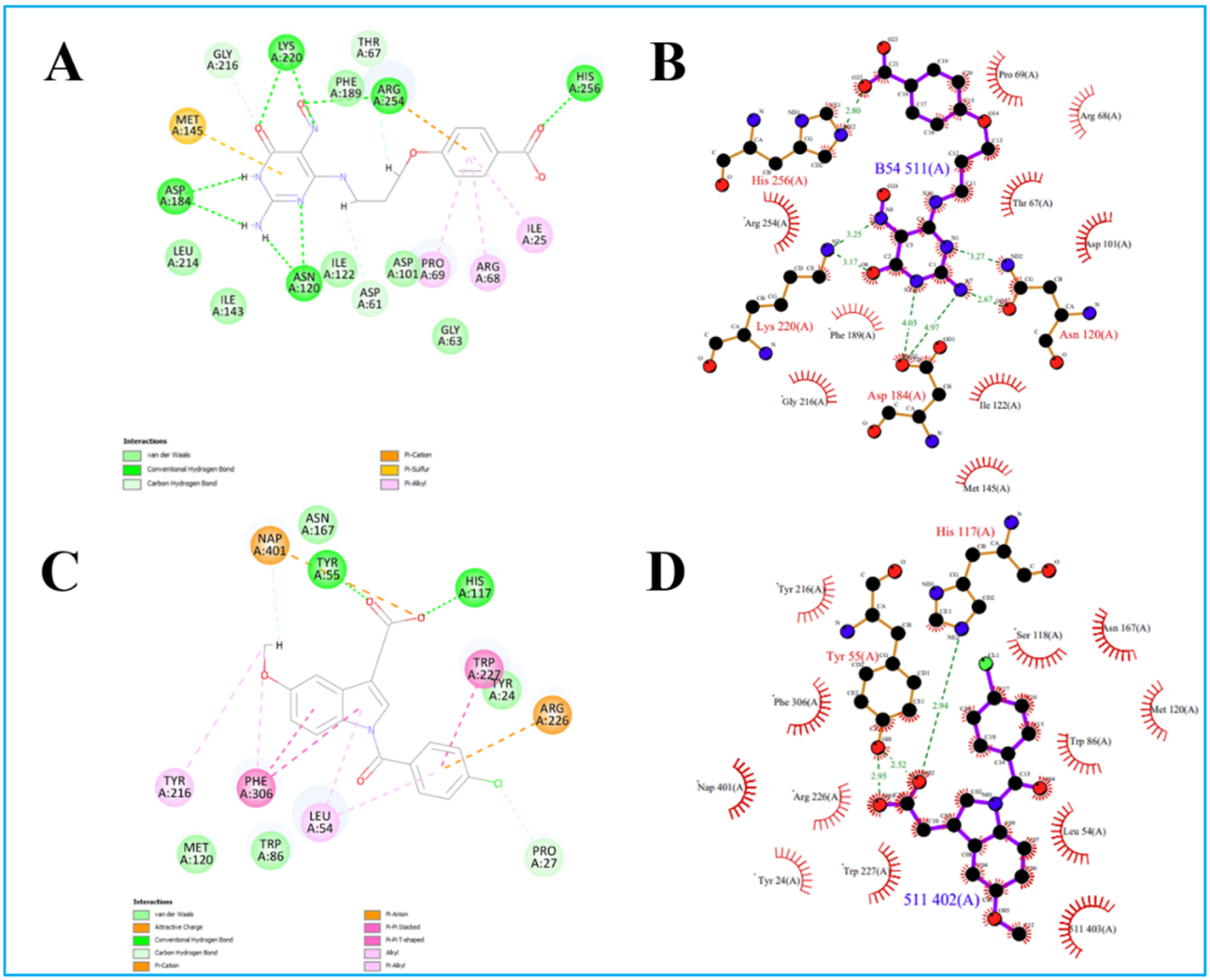

Fig. 10 (A and B) 2D interaction plots of the redocked pose and the co-crystallized pose of B54, respectively, with 3H23. (C and D) 2D interaction plots of the redocked pose and the co-crystallized pose of 511, respectively, with 4DBW.

and 511 in 4DBW to validate the docking protocol. From the redocking calculations, it was observed that B54 (4-{3-[(2-amino-5-nitroso-6-oxo-1,6-dihydropyrimidin-yl)amino]propoxy} benzoic acid) and 511 ([1-(4-chlorobenzoyl)-5-methoxy-1*H*-indol-3-yl]acetic acid) displayed RMSD values of 0.84 Å and 0.50 Å, respectively, with the redocking score of −11.78 kcal mol^{-1} and −13.35 kcal mol^{-1}, respectively (Fig. S23). Thus, from the RMSD values obtained from the redocking studies, a good agreement between the redocked and experimental poses was observed. Moreover, it was also noted that B54 forms hydrogen bonds with Asn120, Asp184, Lys220, and His256, while 511 showed hydrogen bond interactions with Tyr55 and His117. From the 2D interaction pose of redocked B54 and 511, it was observed that both molecules displayed all experimentally reported interactions, thus validating our software (Fig. 10).

2.7.3.2 Molecular docking analysis of the selected molecules. Molecular docking was performed on the selected compounds (**3a–3i**) to evaluate the binding affinity and interaction profiles against the protein targets 3H23 and 4DBW. Molecular docking analysis revealed that all nine molecules were able to dock in the active site of both enzymes (Fig. 11 and 12). Their 3D and 2D interaction plots are shown in Fig. 13 and 14. A graphical overview of the docking outcomes of all derivatives with target proteins 3H23 & 4DBW is demonstrated in Fig. 15. 3D interactions of all 9 scaffolds are presented as videos in the SI as Video S1 for 3H23 and Video S2 for 4DBW.

On observing the docking findings as shown in Table 5, it is clear that in the case of 3H23, **3a** showed the highest docking score of **−16.07** kcal mol^{-1}, followed by **3i** (−13.47 kcal mol^{-1}), **3e** (−13.02 kcal mol^{-1}), **3c** (−11.95 kcal mol^{-1}), **3d** (−11.29 kcal mol^{-1}), **3h** (−11.27 kcal mol^{-1}), **3g** (−09.67 kcal mol^{-1}), **3f** (−09.14 kcal mol^{-1}), and **3b** (−09.01 kcal mol^{-1}). In case of docking with 4DBW, **3c** presented the highest docking score of **−19.29** kcal mol^{-1}, followed by **3d** (−18.01 kcal mol^{-1}), **3a** (−16.40 kcal mol^{-1}), **3g** (−15.87 kcal mol^{-1}), **3e** (−13.97 kcal mol^{-1}), **3i** (−12.80 kcal mol^{-1}), **3b** (−11.53 kcal mol^{-1}), **3f** (−10.57 kcal mol^{-1}), and **3h** (−09.38 kcal mol^{-1}). However, on

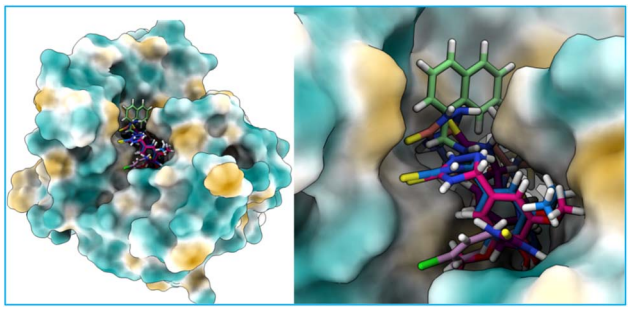

Fig. 11 3D representation of 3H23 docked with all synthesized molecules.

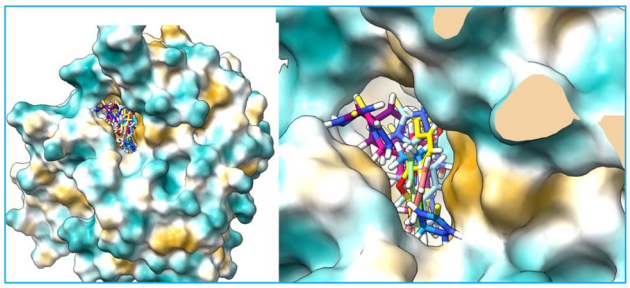

Fig. 12 3D representation of 4DBW docked with all synthesized molecules.

comparing the docking outcome with the redocking score of the respective enzyme, it was observed that molecules **3a**, **3e** and **3c** were commonly docked in both enzymes. In 3H23, the molecule **3a** forms hydrogen bonding with Pro69 and Arg254, pi–pi

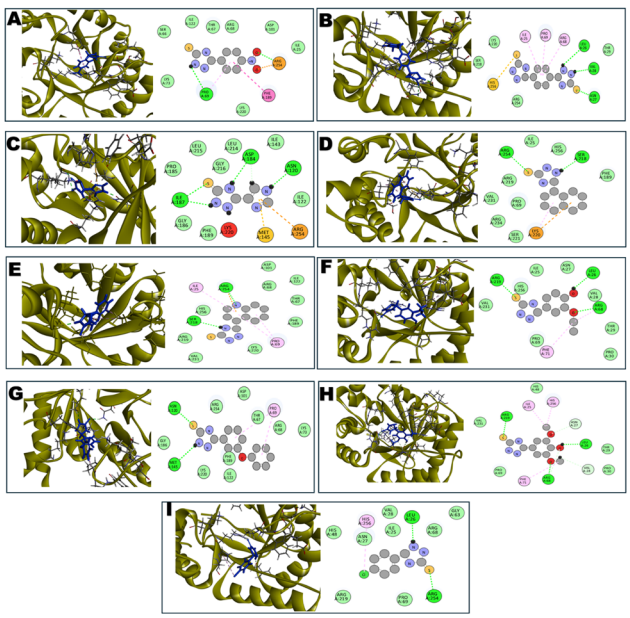

Fig. 13 3D and 2D representations of 3H23 docked with 9 selected molecules. (A) 3H23-**3a**, (B) 3H23-**3i**, (C) 3H23-**3e**, (D) 3H23-**3c**, (E) 3H23-**3d**, (F) 3H23-**3h**, (G) 3H23-**3g**, (H) 3H23-**3f**, (I) 3H23-**3b**.

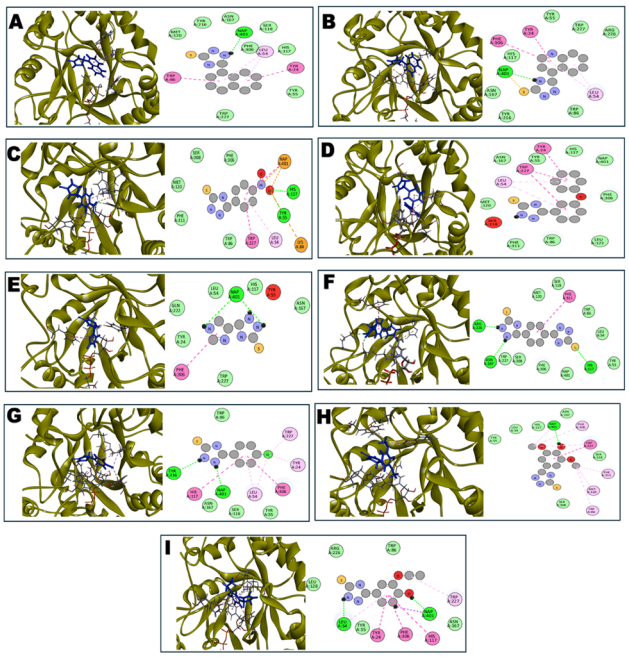

Fig. 14 3D and 2D representations of 4DBW docked with 9 selected molecules. (A) 4DBW-**3c**, (B) 4DBW-**3d**, (C) 4DBW-**3a**, (D) 4DBW-**3g**, (E) 4DBW-**3e**, (F) 4DBW-**3i**, (G) 4DBW-**3b**, (H) 4DBW-**3f**, (I) 4DBW-**3h**.

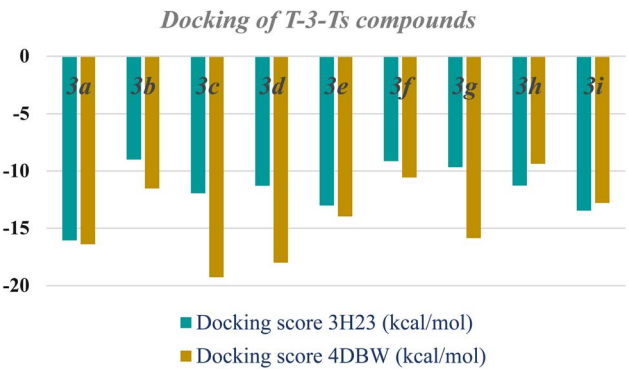

Fig. 15 Visual representation of docking results of all the synthesized compounds.

interactions with Phe189, and hydrophobic interactions with the amino acids Ile25, Lys73, and Asp101. Also, molecule **3e** forms hydrogen bonding with Asn120, Asp184, and Ile187, and hydrophobic interactions with Ile122, Ile143, Pro185, Gly186, Phe189, Leu214, Leu215, and Gly216. Likewise, molecule **3c** form hydrogen bonding with Ser218, Lys220, and Arg254, and hydrophobic contacts with Ile25, Pro69, Phe189, Arg219, Ser221, Val231, Arg234, and His256. Additionally, various types of hydrogen bonding, hydrophobic, pi–pi, and pi–alkyl interactions were observed in 2D interaction plots (Table 6). Moreover, Leu26 and Arg254 are the most common amino acids forming hydrogen bonds with the nine docked candidates (Fig. 13 and S24). Hydrophobic interactions were observed *via* amino acids Ile25, Val28, Arg68, Ile122, Lys220, and His256. These residues provide a stable, non-polar environment for the

Table 5 List of docking scores of nine synthesized 5-phenyl-1,2,4-triazolidine derivatives with 3H23 and 4DBW PDBs

3H23		4DBW	
Molecules	Docking score (kcal mol^{-1})	Molecules	Docking score (kcal mol^{-1})
3a	−16.07	**3c**	−19.29
3i	−13.47	**3d**	−18.01
3e	−13.02	**3a**	−16.40
3c	−11.95	**3g**	−15.87
3d	−11.29	**3e**	−13.97
3h	−11.27	**3i**	−12.80
3g	−09.67	**3b**	−11.53
3f	−09.14	**3f**	−10.57
3b	−09.01	**3h**	−09.38

ligand to bind. These interactions help the ligands to bind in the active site of the enzyme, 17β-dehydrogenase.

In this case of 4DBW, the NADP (Nap401) cofactor played an important role in stabilizing the ligand binding. Compound **3c** showed hydrogen bonding interactions with Nap401, pi–alkyl interactions with Leu54, pi–pi interactions with Tyr24, and Trp86, and hydrophobic interactions with Tyr55, His117, Ser118, Met120, Asn167, Tyr216, Trp227, and Phe306, crucial residues known to mediate NADP recognition. Molecule **3a** showed hydrogen bonding with Tyr55, and His117, pi–pi interactions with Trp227, and Nap401, Pi-alkyl bonding with Leu54, and hydrophobic interactions with Trp86, Met120, Phe306, Ser308, and Phe311. Molecule **3e** forms hydrogen bonding with Nap401 and hydrophobic contacts with Tyr24, Leu54, His117, Asn167, Gln222, and Trp227. Additionally, from the 2D interaction plot of 4DBW, it is observed that hydrogen bonding is formed *via* Leu54, Tyr55, His117, and Tyr216 (Fig. 14 and S25). Hydrophobic interactions are formed *via* Tyr55, Trp86, His117, Ser118, Met120, Asn167, Phe306, Ser308, and His117. The pi–pi interactions are formed *via* Tyr24, Trp224, and Phe306, and pi–alkyl interactions are formed *via* Leu54 and Trp227. The presence of these interactions highlights that the molecules may act as competitive inhibitors, mimicking the binding of NADP. Overall, from the docking outcome, the presence of important interactions demonstrated strong

Table 6 List of various types of interactions reported in the docked complexes of 3H23 and 4DBW[a]

	H-bonding	Hydrophobic	Pi–pi	Pi–alkyl
3H23				
3a	Pro69, and Arg254	Ile25, Asp101, Arg68, Thr67, Ile122, Ser66, Lys73, and Lys220	Phe189	Pro69
3i	Leu26, Val28, and Asn27	Thr29, Arg254, Ser218, and Lys220	—	Ile25, Pro69, and Arg68
3e	Ile187, Asp184, and Asn120	Ile122, Phe189, Gly186, Pro185, Leu215, Gly216, Leu214, and Ile143	—	—
3c	Ser218, and Arg254	Phe189, His256, Ile25, Arg219, Pro69, Val231, Arg234, and Ser221	—	Lys220
3d	Ser218, and Arg254	Asp101, Thr67, Phe189, Lys220, Val231, Arg219, His256, Arg68, and Ile122	—	Ile25, and Pro69
3h	Arg219, Leu26, and Arg68	Thr29, Pro30, Pro69, Val231, His256, Ile25, Asn27, and Val28	—	Phe71, and Arg68
3g	Asn120, and Met145	Lys73, Ile122, Lys220, Gly186, Arg254, Asp101, and Arg68	—	Pro69
3f	Leu26, Arg68, and Arg219	Thr29, Pro30, Pro69, Val231, and His48	—	His256, Ile25, and Phe71
3b	Leu26, and Arg254	Arg68, Gly63, Ile25, Val28, Asn27, His48, Arg219, and Pro69	—	His256
4DBW				
3c	Nap401	His117, Trp227, Tyr55, Met120, Tyr216, Asn167, Phe306, and Ser118	Tyr24, and Trp86	Leu54
3d	Nap401	Trp86, Tyr216, Asn167, His117, Tyr55, Trp227, and Arg226	Tyr24, and Phe306	Leu54
3a	His117, and Tyr55	Trp86, Phe311, Met120, Ser308, and Phe306	Trp227, and Nap401	Leu54
3g	—	Leu122, Trp86, Phe311, Met120, Asn167, Tyr55, His117, Nap401, and Phe306	Tyr24, and Trp227	Leu54
3e	Nap401	Trp227, Tyr24, Gln222, Leu54, His117, and Asn167	—	—
3i	His117, Asn307, and Arg226	Tyr55, Nap401, Phe306, Ser308, Trp227, Met120, Ser118, Trp86, and Leu54	Phe311	—
3b	Tyr216, Nap401	Asn167, Trp86, Ser118, and Tyr55	Phe306, and His117	Trp227, Tyr24, & Leu54
3f	Nap401	Ser308, Ser118, Tyr55, Leu54, His117, and Asn167	Trp227	Phe311, Met120, Trp86, Trp227, & Phe306
3h	Leu54, Nap401	Leu128, Asn167, Trp86, and Arg226	Tyr24, Phe306, and His117	Trp227, & Leu54

[a] Nap is the cofactor.

binding affinity against the two selected enzymes, thus highlighting their potential as promising 17β-dehydrogenase and pterin deaminase inhibitors.

3 Experimental

3.1. Synthesis of KP-CQDs

For the synthesis of KP-CQDs, drop-down red-colored flowers of *Kigelia pinnata* were collected from the local garden (Gulabbagh, Udaipur, Rajasthan, India). The collected flowers were thoroughly washed 3 to 4 times with lukewarm water to remove dust. After cleaning, they were dried for about 3 days in the shade. The dried flowers were then ground into a fine powder (brown powder). Then, 4.0 g of powder was dissolved in 80 mL of DI water and stirred for 30 min. Then, the resulting solution was transferred to a 150 mL Teflon-lined stainless-steel autoclave and was placed in a hot air oven and heated for 12 h at 160 °C. After that, the autoclave was allowed to cool to RT naturally. The obtained solution was then centrifuged to separate the suspension, followed by filtration using a 0.45 μm filter membrane. The final product was a clear, dark brown color solution (62 mL), which was named KP-CQDs and stored in a glass vial under refrigerated conditions. Fig. 16 presents the step-wise synthesis of KP-CQDs.

To determine the yield and concentration of the synthesized KP-CQDs, a previously reported method was followed.[59,60] The entire 62 mL of KP-CQD solution was transferred to a pre-weighed 100 mL beaker. After accurately recording the initial mass, the solvent was evaporated completely by drying the sample in an oven at 80 °C. The final weight of the beaker containing the dried KP-CQDs was then measured. The yield (%) and concentration (mg mL^{-1}) were calculated using the following equations, and a detailed calculation is given in the SI.

Yield (%) = {Mass of dried KP-CQDs obtained (g)/Mass of biomass used (g)} × 100.

Concentration (mg mL^{-1}) = Mass of dried KP-CQDs (mg)/Volume of KP-CQD solution (mL).

[Mass of dried KP-CQDs = Final beaker weight − Initial beaker weight].

The yield of the KP-CQDs was found to be **27.375**% and the concentration was found to be **17.661** mg mL^{-1}.

3.2. General synthetic method for 1,2,4-triazolidines

A mixture of substituted aldehyde (1 mmol) and TCS (1 mmol) was stirred with KP-CQDs (0.50 mL) in a 3 mL ethanol–water combination (1 : 4) at RT. The reaction completion was checked by TLC (hexane-ethyl acetate, 7 : 3). Upon completion, the precipitated product was separated by simple filtration, thoroughly washed with H_2O, and dried in an oven at 60 °C. The catalyst + solvent mixture (found as the filtrate) was reused directly in subsequent reactions without any purification step.

For the synthesis of **3i**, the starting material ratios were adjusted as follows:

Synthesis of **3i**: terephthaldehyde (0.5 mmol) was reacted with thiosemicarbazide (1.0 mmol) to produce a bis-triazolidine product.

3.3. ADMET studies and molecular docking calculations

The integration of computational studies, such as molecular docking and ADMET analysis, has significantly advanced the understanding of the disease mechanism and helps to identify potential drug targets and evaluate the development of the

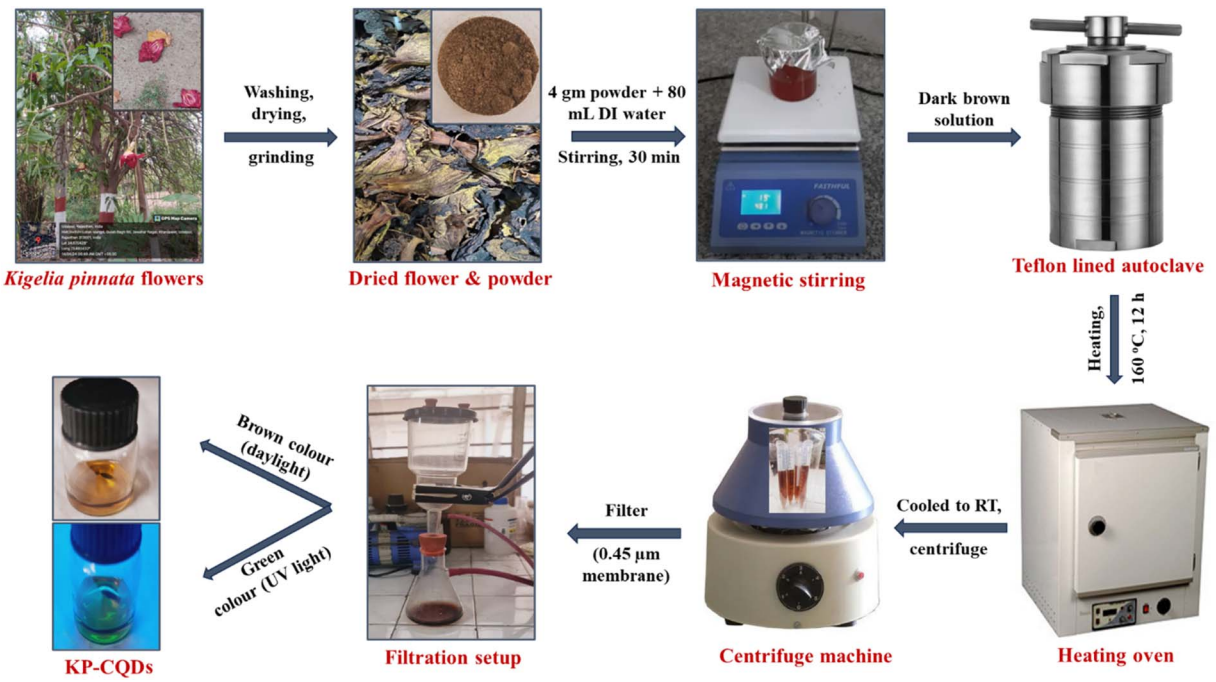

Fig. 16 Step-wise hydrothermal synthesis of KPCQDs from *Kigelia pinnata* flowers.

molecule with optimized efficacy and safety profiles.[61] The web-based AdmetSAR 3.0 was employed to study the pharmacokinetics and physicochemical properties of the nine synthesized molecules.[58] This tool predicts the pharmacokinetic properties, such as absorption, distribution, metabolism, excretion, and toxicity (ADMET). Under ADMET, parameters, such as Caco-2 permeability, human intestinal absorption (HIA), blood–brain barrier (BBB), plasma protein binding (PPB), CYP2B6 inhibitor, human liver microsome stability (HLM), renal clearance (CLr), half-life (T50), neurotoxicity and drug-induced liver injury (DILI) were estimated and compared with acceptable range as mentioned in Table S2. These parameters play a crucial role in predicting drug behavior in the body. Moreover, the physicochemical properties, such as molecular weight (MW), total polar surface area (TPSA), and Lipinski's rule, were also studied.

Molecular docking was conducted to study their interacting capability with the enzymes predicted *via* PASS online. Thus, molecular docking played a critical role in the field of drug design.[62] In the present work, molecular docking was performed by using the FlexX module[63] of the SeeSAR software v13.1.1 (ref. 64) to estimate the binding score. The docking protocol used in the current study was validated by conducting redocking on the selected inhibitors B54 (3H23) and 511 (4DBW) co-crystallized in the respective proteins. The selected PDBs, 3H23 and 4DBW, were prepared using the Protein Editor mode of SeeSAR v13.1.1.[64] The protein preparation step involves the removal of water, the addition of missing side chains, and the incorporation of hydrogens. After protein preparation, each complex was subjected to a binding site mode, where the co-crystallized ligand is extracted, and the binding site is confirmed at that pocket. The protein that contains the binding site was subjected to docking mode, which utilizes the FlexX[63] module to estimate the docking score. This module calculates the docking score based on the incremental construction-based algorithm. Here, ligands are divided into smaller fragments and positioned at multiple locations within the binding pocket and evaluated using a rapid, simple pre-scoring scheme. While docking, each molecule generates ten poses, from which the top-scoring pose was selected. Post-docking analyses, such as interaction studies, were conducted using the Discovery Studio visualizer.[65]

3.4. Spectral data of synthesized compounds

3.4.1. 5-(4-Nitrophenyl)-1,2,4-triazolidine-3-thione (3a). Shiny yellow powder; 97% yield; M.P. 221–224 °C;[66] ^{1}H NMR (400 MHz, DMSO-d_6) δ 11.69 (s, 1H, NH), 8.39 (s, 1H, NH), 8.25 (s, 1H, NH), 8.18 (d, J = 9.2 Hz, 2H, Ar–H), 8.08–8.06 (m, 2H, Ar–H), 8.04 (s, 1H, CH). ^{13}C NMR (101 MHz, DMSO-d_6) δ 178.93, 148.07, 141.27, 140.03, 128.70, 124.33. $C_8H_8N_4O_2S$ [m/z] 224.0368.

3.4.2. 5-(4-Chlorophenyl)-1,2,4-triazolidine-3-thione (3b). White powder; 96% yield; M.P. 204–206 °C;[25] ^{1}H NMR (400 MHz, DMSO-d_6) δ 11.46 (s, 1H, NH), 8.22 (s, 1H, NH), 8.05 (s, 1H, NH), 7.98 (s, 1H, CH), 7.81–7.79 (m, 2H, Ar–H), 7.42–7.40 (m, 2H, Ar–H). ^{13}C NMR (101 MHz, DMSO-d_6) δ 178.54, 141.33, 134.74, 133.71, 129.48, 129.22. $C_8H_8ClN_3S$ [m/z] 213.0127.

3.4.3. 5-(Naphthalen-1-yl)-1,2,4-triazolidine-3-thione (3c). Off-white fluffy powder; 89% yield; M.P. 209–211 °C;[67] ^{1}H NMR (400 MHz, DMSO-d_6) δ 11.45 (s, 1H, NH), 8.88 (s, 1H, CH), 8.32–8.29 (m, 2H, NH), 8.19 (dd, J = 7.3, 0.8 Hz, 1H, Ar–H), 7.97–7.95 (m, 3H, Ar–H), 7.63–7.59 (m, 1H, Ar–H), 7.56–7.51 (m, 2H, Ar–H). ^{13}C NMR (101 MHz, DMSO-d_6) δ 178.35, 141.44, 133.91, 130.99, 130.76, 129.76, 129.37, 127.79, 126.68, 126.28, 126.11, 123.36. $C_{12}H_{11}N_3S$ [m/z] 229.0674.

3.4.4. 5-(Quinolin-4-yl)-1,2,4-triazolidine-3-thione (3d). Off-white powder; 89% yield; M.P. 232–235 °C^{new}; ^{1}H NMR (400 MHz, DMSO-d_6) δ 11.66 (s, 1H, NH), 8.89 (d, J = 4.6 Hz, 1H, Ar–H), 8.84 (s, 1H, CH), 8.45 (s, 1H, NH), 8.25 (d, J = 8.3 Hz, 1H, Ar–H), 8.19 (s, 1H, NH), 8.14 (d, J = 4.6 Hz, 1H, Ar–H), 8.04 (d, J = 8.3 Hz, 1H, Ar–H), 7.79–7.75 (m, 1H, Ar–H), 7.69–7.65 (m, 1H, Ar–H)). ^{13}C NMR (101 MHz, DMSO-d_6) δ 179.00, 150.64, 148.90, 138.31, 137.82, 130.37, 130.07, 127.93, 125.58, 123.52, 118.46. HRMS for $C_{11}H_{10}N_4S$ (M + H$^+$); calculated: 231.0660 and found: 231.0705.

3.4.5. 5-(1*H*-imidazol-4-yl)-1,2,4-triazolidine-3-thione (3e). Shiny beige powder; 82% yield; M.P. 190–193 °C^{new}; ^{1}H NMR (400 MHz, DMSO-d_6) δ 12.45 (s, 1H, NH of imidazole), 11.36 (s, 1H, NH), 8.14 (s, 1H, NH), 7.90 (s, 2H, Ar–H), 7.76 (s, 1H, CH), 7.26 (br, 1H, NH). HRMS for $C_5H_7N_5S$ (M + H$^+$); calculated: 170.0456 and found: 170.0500.

3.4.6. 5-(4-Hydroxy-3,5-dimethoxyphenyl)-1,2,4-triazolidine-3-thione (3f). Fluffy white powder; 90% yield; M.P. 136–139 °C^{new}; ^{1}H NMR (400 MHz, DMSO-d_6) δ 11.30 (s, 1H, NH), 8.80 (br, 1H, OH), 8.12 (s, 1H, NH), 7.98 (s, 1H, NH), 7.87 (s, 1H, CH), 7.00 (s, 2H, Ar–H), 3.76 (s, 6H, OCH_3). ^{13}C NMR (101 MHz, DMSO-d_6) δ 177.83, 148.56, 143.41, 138.12, 124.87, 105.32, 56.60. HRMS for $C_{10}H_{13}N_3O_3S$ (M + H$^+$); calculated: 256.0711 and found: 256.0757.

3.4.7. 5-(3-Phenoxyphenyl)-1,2,4-triazolidine-3-thione (3g). White fluffy powder; 92% yield; M.P. 201–203 °C;[67] ^{1}H NMR (400 MHz, DMSO-d_6) δ 11.44 (s, 1H, NH), 8.19 (s, 1H, NH), 8.05 (s, 1H, NH), 7.98 (s, 1H, CH), 7.58–7.57 (m, 1H, Ar–H), 7.49 (dd, J = 6.7, 1.1 Hz, 1H, Ar–H), 7.39–7.33 (m, 3H, Ar–H), 7.11–7.07 (m, 1H, Ar–H), 6.97–6.94 (m, 3H, Ar–H)). ^{13}C NMR (101 MHz, DMSO-d_6) δ 178.52, 157.27 (d, J = 7.9 Hz), 141.94, 136.91, 130.85, 130.61, 123.83 (d, J = 13.4 Hz), 120.70, 118.77, 117.81. $C_{14}H_{13}N_3OS$ [m/z] 271.0779.

3.4.8. 5-(3-Ethoxy-4-hydroxyphenyl)-1,2,4-triazolidine-3-thione (3h). White powder; 87% yield; M.P. 172–175 °C;[67] ^{1}H NMR (400 MHz, DMSO-d_6) δ 11.22 (s, 1H, NH), 9.36 (s, 1H, OH), 8.08 (s, 1H, NH), 7.93 (s, 1H, NH), 7.87 (s, 1H, CH), 7.42 (d, J = 1.8 Hz, 1H, Ar–H), 6.97 (dd, J = 8.2, 1.8 Hz, 1H, Ar–H), 6.74 (d, J = 8.1 Hz, 1H, Ar–H), 4.03 (q, J = 7.0 Hz, 2H, CH_2), 1.30 (t, J = 7.0 Hz, 3H, CH_3). ^{13}C NMR (101 MHz, DMSO-d_6) δ 177.81, 149.50, 147.76, 143.43, 126.07, 122.87, 115.73, 110.84, 64.37, 15.24. $C_{10}H_{13}N_3O_2S$ [m/z] 239.0728.

3.4.9. 5,5′-(1,4-Phenylene)bis(1,2,4-triazolidine-3-thione) (3i). White fluffy powder; 90% yield; M.P. 202–204 °C;[25] ^{1}H NMR (400 MHz, DMSO-d_6) δ 11.44 (s, 2H, NH), 8.19 (s, 2H, NH), 8.01 (d, J = 5.3 Hz, 2H of NH + 2H of CH), 7.77 (s, 4H, Ar–H). ^{13}C NMR (101 MHz, DMSO-d_6) δ 178.54, 142.16, 135.92, 128.04. $C_{10}H_{12}N_6S_2$ [m/z] 280.0565.

4 Conclusion

In conclusion, this study presents a green, sustainable, and efficient approach for the synthesis of CQDs using *Kigelia pinnata* flowers as a novel biowaste-derived carbon source. The resulting KP-CQDs were thoroughly characterized using various analytical techniques. FT-IR studies confirmed the presence of surface functionalities such as –COOH and –OH groups, which contribute to their catalytic efficiency. HRTEM analysis revealed an average particle size of 3.78 nm. These KP-CQDs functioned as highly effective, metal-free nanocatalysts for the synthesis of 1,2,4-triazolidine derivatives under mild and eco-friendly conditions. The methodology demonstrated excellent performance with high product yields, short reaction times, catalyst recyclability, and successful gram-scale synthesis with remarkable results.

Furthermore, the synthesized compounds were evaluated for their molecular docking against 17β-dehydrogenase and pterin deaminase, supported by favorable PASS predictions and ADME profiles. Based on the ADMET analysis and docking studies, we can conclude that molecules **3a** and **3c** exhibit the highest therapeutic potential, inhibiting the enzymes involved in pterin catabolism (pterin deaminase) and in steroid hormone biosynthesis (17β-dehydrogenase), respectively. These findings highlight the dual potential of KP-CQDs in green chemistry and the early stage of drug discovery, emphasizing their value in sustainable and medicinally relevant applications.

Consent for publication

Yes, by all authors.

Author contributions

S. T. performed the original research and wrote the manuscript. S. S. helped in editing and revising. N. R. and A. M. performed the docking studies. S. A. contributed to guiding, writing, and revising the manuscript.

Conflicts of interest

The authors confirmed that this article has no conflict of interest.

Abbreviations

CQDs	Carbon quantum dots
KP-CQDs	*Kigelia pinnata* flower-derived CQDs
PASS	Prediction of activity spectra for substances
PEG	Polyethylene glycol
HRTEM	High resolution transmission electron microscopy
EDX	Energy dispersive X-ray spectroscopy
FT-IR	Fourier transfer infrared spectroscopy
XRD	X-ray diffraction
SAED	Selected area electron diffraction
PDB	Protein data bank
TSC	Thiosemicarbazide
T-3-Ts	1,2,4-Triazolidine-3-thione
ADMET	Absorption, distribution, metabolism, excretion, & toxicity
TLC	Thin layer chromatography
NMR	Nuclear magnetic resonance
HRMS	High resolution mass spectroscopy
RCSB	Research collaboratory for structural bioinformatics

Data availability

The data supporting this article have been included as part of the supplementary information (SI).

Supplementary information: the supporting information is available for readers in the supplementary file, which includes ^{1}H, ^{13}C NMR and mass spectra of the synthesized compounds. See DOI: **https://doi.org/10.1039/d5na00734h**.

Acknowledgements

The authors are thankful to the Department of Chemistry, MLSU, Udaipur, for providing research facilities. They are also grateful to IIT Jammu, IIT Mumbai, SAIF-Chandigarh, and the Department of Physics for analyzing HRMS, HRTEM, UV-Vis, fluorescence, EDX, and XRD, respectively. S. Agarwal and S. Teli acknowledge DST-ANRF, SURE (No. SUR/2022/001312) for financial support. S. Agarwal also sincerely acknowledges the Ministry of Education, SPD-RUSA, Rajasthan, for providing the NMR facility under RUSA 2.0, Research and Innovation project (File no./RUSA/GEN/MLSU/2020/6394).

References

1 F. D. Guerra, M. F. Attia, D. C. Whitehead and F. Alexis, Nanotechnology for Environmental Remediation: Materials and Applications, *Molecules*, 2018, **23**(7), 1760.
2 M. Ajaz, W. Rasool and A. Mahmood, Comprehensive Review of Nanotechnology: Innovations and Multidisciplinary Applications: Comprehensive Review of Nanotechnology, *Futuristic Biotechnol.*, 2024, **4**(01), 12–18.
3 O. S. Ayanda, A. O. Mmuoegbulam, O. Okezie, N. I. Durumin Iya, S. a. E. Mohammed, P. H. James, A. B. Muhammad, A. A. Unimke, S. A. Alim, S. M. Yahaya, A. Ojo, T. O. Adaramoye, S. K. Ekundayo, A. Abdullahi and H. Badamasi, Recent progress in carbon-based nanomaterials: critical review, *J. Nanopart. Res.*, 2024, **26**(5), 106.
4 A. O. Egbedina, O. P. Bolade, U. Ewuzie and E. C. Lima, Emerging trends in the application of carbon-based materials: A review, *J. Environ. Chem. Eng.*, 2022, **10**(2), 107260.
5 A. Vijeata, G. R. Chaudhary, S. Chaudhary, A. A. Ibrahim and A. Umar, Recent advancements and prospects in carbon-based nanomaterials derived from biomass for environmental remediation applications, *Chemosphere*, 2024, **357**, 141935.

6 S. Teli, P. Teli, S. Soni, L. K. Agarwal, and S. Agarwal, 19 - Quantum dots-based sensors to detect environmental contaminants, In *Nanotechnology-based Sensors for Detection of Environmental Pollution*, ed. F. M. Policarpo Tonelli, A. Roy, M. Ozturk,and H. C. A. Murthy, Elsevier, 2024, pp. 371–407.
7 D. L. Zhao and T.-S. Chung, Applications of carbon quantum dots (CQDs) in membrane technologies: A review, *Water Res.*, 2018, **147**, 43–49.
8 S. Teli, S. Shivani and S. Agarwal, Harnessing bioinspired carbon quantum dots: a six-year odyssey in synthesis and catalytic revolution, *Crit. Rev. Solid State Mater. Sci.*, 2024, 1–62.
9 S. Teli, S. Soni, P. Teli, N. Sahiba and S. Agarwal, Unlocking the potential of Ficus religiosa tree bark-derived biochar sulfonic acid: a journey from synthesis and characterization to its astonishing catalytic role in green synthesis of perimidines, *Res. Chem. Intermed.*, 2024, **50**(3), 1475–1495.
10 A. Mermer, T. Keles and Y. Sirin, Recent studies of nitrogen containing heterocyclic compounds as novel antiviral agents: A review, *Bioorg. Chem.*, 2021, **114**, 105076.
11 W. M. Huggins, B. M. Minrovic, B. W. Corey, A. C. Jacobs, R. J. Melander, R. D. Sommer, D. V. Zurawski and C. Melander, 1,2,4-Triazolidine-3-thiones as Narrow Spectrum Antibiotics against Multidrug-Resistant Acinetobacter baumannii, *ACS Med. Chem. Lett.*, 2017, **8**(1), 27–31.
12 N. U. Hebbar, P. S. Hebbar, P. P. Rathode, B. Negalura, A. Hiremath, P. Gudimani, L. A. Shastri, S. K. Praveen Kumar, A. J. Kadapure and S. Joshi, Synthesis, characterization of 1,2,4-triazolidine-3-thione tethered beta-aryl butanoic acid and butanoate derivatives as potent antimicrobial and antioxidant agents and their molecular docking studies, *J. Mol. Struct.*, 2023, **1280**, 135003.
13 F. Shaikh, S. L. Shastri, N. S. Naik, R. Kulkarni, J. M. Madar, L. A. Shastri, S. D. Joshi and V. Sunagar, Synthesis, Antitubercular and Antimicrobial Activity of 1,2,4-Triazolidine-3-thione Functionalized Coumarin and Phenyl Derivatives and Molecular Docking Studies, *ChemistrySelect*, 2019, **4**(1), 105–115.
14 H. Adibi, L. Hosseinzadeh, M. Mahdian, A. Foroumadi, M. A. Zolfigol and S. Mallakpour, Synthesis of 7-Substituted Fluoroquinolone Derivatives Containing Triazolidine Dione Moiety and *In Vitro* Evaluation of their Cytotoxic Effects, *J. Rep. Pharm. Sci.*, 2013, **2**(1), 75–82.
15 V. Kanagarajan, J. Thanusu and M. Gopalakrishnan, Synthesis and *in vitro* microbiological evaluation of novel 2,4-diaryl-3-azabicyclo[3.3.1]nonan-9,5′-spiro-1′,2′,4′-triazolidine-3′-thiones, *Med. Chem. Res.*, 2012, **21**(12), 3965–3972.
16 J. T. Witkowski, R. K. Robins, G. P. Khare and R. W. Sidwell, Synthesis and antiviral activity of 1,2,4-triazole-3-thiocarboxamide and 1,2,4-triazole-3-carboxamidine ribonucleosides, *J. Med. Chem.*, 1973, **16**(8), 935–937.
17 R. Spinelli, I. Sanchis, F. M. Aimaretti, A. M. Attademo, M. Portela, M. V. Humpola, G. G. Tonarelli and A. S. Siano, Natural Multi-Target Inhibitors of Cholinesterases and Monoamine Oxidase Enzymes with Antioxidant Potential from Skin Extracts of Hypsiboas cordobae and Pseudis minuta (Anura: Hylidae), *Chem. Biodiversity*, 2019, **16**(1), e1800472.
18 E. Andrade-Jorge, J. Bribiesca-Carlos, F. J. Martínez-Martínez, M. A. Soriano-Ursúa, I. I. Padilla-Martínez and J. G. Trujillo-Ferrara, Crystal structure, DFT calculations and evaluation of 2-(2-(3,4-dimethoxyphenyl)ethyl) isoindoline-1,3-dione as AChE inhibitor, *Chem. Cent. J.*, 2018, **12**(1), 74.
19 R. Alvarez, S. Velazquez, A. San-Felix, S. Aquaro, E. D. Clercq, C.-F. Perno, A. Karlsson, J. Balzarini and M. J. Camarasa, 1,2,3-Triazole-[2,5-Bis-O-(tert-butyldimethylsilyl)-.beta.-D-ribofuranosyl]-3'-spiro-5''-(4''-amino-1'',2''-oxathiole 2'',2''-dioxide) (TSAO) Analogs: Synthesis and Anti-HIV-1 Activity, *J. Med. Chem.*, 1994, **37**(24), 4185–4194.
20 A. H. Banday, S. A. Shameem, B. D. Gupta and H. M. S. Kumar, D-ring substituted 1,2,3-triazolyl 20-keto pregnenanes as potential anticancer agents: Synthesis and biological evaluation, *Steroids*, 2010, **75**(12), 801–804.
21 D. R. Buckle, C. J. M. Rockell, H. Smith and B. A. Spicer, Studies on 1,2,3-triazoles. 13. (Piperazinylalkoxy)-[1] benzopyrano[2,3-d]-1,2,3-triazol-9(1H)-ones with combined H1-antihistamine and mast cell stabilizing properties, *J. Med. Chem.*, 1986, **29**(11), 2262–2267.
22 C. S. Wisniewski, Rufinamide: A New Antiepileptic Medication for the Treatment of Seizures Associated with Lennox-Gastaut Syndrome, *Ann. Pharmacother.*, 2010, **44**(4), 658–667.
23 A. C. Cole, J. L. Jensen, I. Ntai, K. L. T. Tran, K. J. Weaver, D. C. Forbes and J. H. Davis, Novel Brønsted Acidic Ionic Liquids and Their Use as Dual Solvent−Catalysts, *J. Am. Chem. Soc.*, 2002, **124**(21), 5962–5963.
24 S. Y. Khatavi and K. Kantharaju, Waste to wealth: agro-waste catalyzed green method synthesis of 5-aryl-1, 2, 4-triazolidine-3-thiones and 1, 2, 4-triazospiro-3-thiones, *Org. Commun.*, 2021, **14**(3), 240–254.
25 L. B. Masram, S. S. Salim, A. B. Barkule, Y. U. Gadkari and V. N. Telvekar, An efficient and expeditious synthesis of 1, 2, 4-triazolidine-3-thiones using meglumine as a reusable catalyst in water, *J. Chem. Sci.*, 2022, **134**(3), 94.
26 M. Mane and D. Pore, A novel one pot multi-component strategy for facile synthesis of 5-aryl-[1, 2, 4] triazolidine-3-thiones, *Tetrahedron Lett.*, 2014, **55**(48), 6601–6604.
27 P. B. Patil, J. D. Patil, S. N. Korade, S. D. Kshirsagar, S. P. Govindwar and D. M. Pore, An efficient synthesis of anti-microbial 1, 2, 4-triazole-3-thiones promoted by acidic ionic liquid, *Res. Chem. Intermed.*, 2016, **42**, 4171–4180.
28 S. N. Korade, J. D. Patil and D. M. Pore, Novel task-specific ionic liquid for room temperature synthesis of spiro-1, 2, 4-triazolidine-3-thiones, *Monatsh. Chem.*, 2016, **147**, 2143–2149.
29 D. M. Pore, P. G. Hegade, M. M. Mane and J. D. Patil, The unprecedented synthesis of novel spiro-1, 2, 4-triazolidinones, *RSC Adv.*, 2013, **3**(48), 25723–25726.

30 R. Ramesh and A. Lalitha, PEG-assisted two-component approach for the facile synthesis of 5-aryl-1, 2, 4-triazolidine-3-thiones under catalyst-free conditions, *RSC Adv.*, 2015, **5**(63), 51188–51192.
31 E. M. Sharshira, R. I. El Sokkary and N. Morsy, Synthesis and antimicrobial evaluation of some heterocyclic compounds from 3-aryl-1-phenyl-1H-pyrazole-4-carbaldehydes, *Z. Naturforsch. B Chem. Sci.*, 2018, **73**(6), 389–397.
32 P. G. Mahajan, N. C. Dige, B. D. Vanjare, H. Raza, M. Hassan, S.-Y. Seo, C.-H. Kim and K. H. Lee, Synthesis and biological evaluation of 1, 2, 4-triazolidine-3-thiones as potent acetylcholinesterase inhibitors: *in vitro* and *in silico* analysis through kinetics, chemoinformatics and computational approaches, *Mol. Diversity*, 2020, **24**, 1185–1203.
33 Z. Pourkarim and M. Nikpassand, Synthesis, characterization and application of Fe3O4@ SiO2@ Tannic acid nanoparticles: A novel and magnetically recyclable catalyst for one-pot synthesis of novel 5-pyrazolin-1, 2, 4-triazolidine-3-ones (thiones), *J. Mol. Struct.*, 2020, **1217**, 128433.
34 P. P. Bardapurkar, S. S. Shewale, S. A. Arote, S. S. Pansambal and N. P. Barde, Effect of precursor pH on structural, magnetic and catalytic properties of CoFe 2 O 4@ SiO 2 green nanocatalyst, *Res. Chem. Intermed.*, 2021, **47**, 1919–1939.
35 S. S. Salim, L. B. Masram, Y. U. Gadkari, A. B. Barkule and V. N. Telvekar, Tartaric Acid as an Expeditious and Green Catalyst for the Synthesis of 1, 2, 4-Triazolidine-3-thiones in an Aqueous Medium, *Org. Prep. Proced. Int.*, 2023, **55**(6), 584–590.
36 P. J. Patil, G. D. Salunke, M. B. Deshmukh, S. P. Hangirgekar, D. R. Chandam and S. A. Sankpal, Thiamine Hydrochloride Catalyzed Synthesis of 1, 2, 4-Triazolidine-3-thiones in Aqueous Medium, *ChemistrySelect*, 2019, **4**(45), 13071–13078.
37 N. Nami and S. Lale Mohammadi, One-Pot Facile Synthesis of New 1, 2, 4- Triazolidine Derivatives Using Sodium Borohydride and Fe3O4 Magnetic Nanoparticles (MNPs), *Int. J. Nanosci. Nanotechnol.*, 2017, **13**(4), 347–357.
38 **https://www.way2drug.com/PassOnline/**.
39 **https://www2.rcsb.org/**.
40 M. P. Romero, F. Alves, M. D. Stringasci, H. H. Buzzá, H. Ciol, N. M. Inada and V. S. Bagnato, One-pot microwave-assisted synthesis of carbon dots and *in vivo* and *in vitro* antimicrobial photodynamic applications, *Front. Microbiol.*, 2021, **12**, 662149.
41 R. Chugh and G. Kaur, Citrus limetta peels derived carbon dots as highly active carbocatalyst for carbon–carbon bond formation, *Clean Technol. Environ. Policy*, 2024, **26**(11), 3907–3919.
42 S. Devi, R. K. Gupta, A. K. Paul and S. Tyagi, Waste carbon paper derivatized Carbon Quantum Dots/(3-Aminopropyl) triethoxysilane based fluorescent probe for trinitrotoluene detection, *Mater. Res. Express*, 2018, **6**(2), 025605.
43 A. Mohammadi, N. Haghnazari and C. Karami, Nano-probe for determination of phenobarbital of green synthesized fluorescent carbon dots using Scrophularia striata, *J. Mater. Sci.: Mater. Electron.*, 2023, **34**(4), 251.
44 K. Dehvari, K. Y. Liu, P.-J. Tseng, G. Gedda, W. M. Girma and J.-Y. Chang, Sonochemical-assisted green synthesis of nitrogen-doped carbon dots from crab shell as targeted nanoprobes for cell imaging, *J. Taiwan Inst. Chem. Eng.*, 2019, **95**, 495–503.
45 A. Dager, T. Uchida, T. Maekawa and M. Tachibana, Synthesis and characterization of mono-disperse carbon quantum dots from fennel seeds: photoluminescence analysis using machine learning, *Sci. Rep.*, 2019, **9**(1), 14004.
46 N. Sudhan, K. Subramani, M. Karnan, N. Ilayaraja and M. Sathish, Biomass-derived activated porous carbon from rice straw for a high-energy symmetric supercapacitor in aqueous and non-aqueous electrolytes, *Energy Fuels*, 2017, **31**(1), 977–985.
47 R. Purbia and S. Paria, A simple turn on fluorescent sensor for the selective detection of thiamine using coconut water derived luminescent carbon dots, *Biosens. Bioelectron.*, 2016, **79**, 467–475.
48 C. Zequine, C. Ranaweera, Z. Wang, S. Singh, P. Tripathi, O. Srivastava, B. K. Gupta, K. Ramasamy, P. Kahol and P. Dvornic, High per formance and flexible supercapacitors based on carbonized bamboo fibers for wide temperature applications, *Sci. Rep.*, 2016, **6**(1), 31704.
49 Y. Li, Q. Zhang, J. Zhang, L. Jin, X. Zhao and T. Xu, A top-down approach for fabricating free-standing bio-carbon supercapacitor electrodes with a hierarchical structure, *Sci. Rep.*, 2015, **5**(1), 14155.
50 S. Kumawat, D. K. Meena, M. Rani, H. S. Mund and G. Arora, Effect of Mg doping at Fe/Cr site on magnetic and optical properties of Gd2FeCrO6 double perovskite, *J. Alloys Compd.*, 2024, **978**, 173339.
51 S. Saini, K. Kumar, P. Saini, D. K. Mahawar, K. S. Rathore, S. Kumar, A. Dandia and V. Parewa, Sustainable synthesis of biomass-derived carbon quantum dots and their catalytic application for the assessment of α, β-unsaturated compounds, *RSC Adv.*, 2022, **12**(50), 32619–32629.
52 H. Nie, M. Li, Q. Li, S. Liang, Y. Tan, L. Sheng, W. Shi and S. X.-A. Zhang, Carbon dots with continuously tunable full-color emission and their application in ratiometric pH sensing, *Chem. Mater.*, 2014, **26**(10), 3104–3112.
53 S. Ding, Y. Gao, B. Ni and X. Yang, Green synthesis of biomass-derived carbon quantum dots as fluorescent probe for Fe3+ detection, *Inorg. Chem. Commun.*, 2021, **130**, 108636.
54 S. Pansambal, S. Ghotekar, R. Oza and K. Deshmukh, Biosynthesis of CuO nanoparticles using aqueous extract of Ziziphus mauritiana L. leaves and their Catalytic performance for the 5-aryl-1, 2, 4-triazolidine-3-thione derivatives synthesis, *Int. J. Sci. Res. Sci. Technol.*, 2019, **5**(4), 122–128.
55 R. A. Sheldon, Metrics of green chemistry and sustainability: past, present, and future, *ACS Sustain. Chem. Eng.*, 2018, **6**(1), 32–48.
56 S. Teli, S. Soni, P. Teli, M. Darji, A. Manhas and S. Agarwal, Synthesis and Application of L-Proline Taurinate as

a Novel Bifunctional Ionic Catalyst for the Highly Efficient Synthesis of 2-Amino-3-Cyano-4H-Pyrans and Pyran-Annulated Heterocycles, *Catal. Lett.*, 2025, **155**(2), 1–22.

57 A. Jayaraman, M. Thandeeswaran, U. Priyadarsini, S. Sabarathinam, K. A. Nawaz and M. Palaniswamy, Characterization of unexplored amidohydrolase enzyme—pterin deaminase, *Appl. Microbiol. Biotechnol.*, 2016, **100**, 4779–4789.

58 F. Cheng, W. Li, Y. Zhou, J. Shen, Z. Wu, G. Liu, P. W. Lee, and Y. Tang, *admetSAR: a Comprehensive Source and Free Tool for Assessment of Chemical ADMET Properties*, ACS Publications, 2012.

59 C. Zapata-Hernandez, G. Durango-Giraldo, M. Gomez-Echeverri, R. Buitrago-Sierra, B. Herrera and K. Cacua, The impact of carbon quantum dots derived from spent coffee grounds on the droplet combustion of diesel/n-butanol blend, *Heliyon*, 2024, **10**(21), e39671.

60 S. Thulasi, A. Kathiravan and M. Asha Jhonsi, Fluorescent carbon dots derived from vehicle exhaust soot and sensing of tartrazine in soft drinks, *ACS Omega*, 2020, **5**(12), 7025–7031.

61 M. Athar, A. Manhas, N. Rana and I. Ahmad, Computational and bioinformatics tools for understanding disease mechanisms, *Biocell*, 2024, **48**(6), 935.

62 P. Solanki, N. Rana, P. C. Jha and A. Manhas, A comprehensive analysis of the role of molecular docking in the development of anticancer agents against the cell cycle CDK enzyme, *Biocell*, 2023, **47**(4), 707–729.

63 M. Rarey, B. Kramer, T. Lengauer and G. Klebe, A fast flexible docking method using an incremental construction algorithm, *J. Mol. Biol.*, 1996, **261**(3), 470–489.

64 BioSolveIT-SeeSAR. **https://www.biosolveit.de/SeeSAR**.

65 D. Visualizer, *Discovery Studio Visualizer. 2*, Accelrys software inc, 2005.

66 P. Teli, S. Soni, S. Teli and S. Agarwal, Unveiling the catalytic potency of a novel hydrazone-linked covalent organic framework for the highly efficient one-pot synthesis of 1, 2, 4-triazolidine-3-thiones, *Nanoscale Adv.*, 2024, **6**(22), 5568–5578.

67 A. Dutta, R. Abha Saikia and A. Jyoti Thakur, A Mechanistic Approach to Liquid-Assisted Mechanochemical Synthesis of 5-Aryl/Spiro-[1, 2, 4]-triazolidine-3-thiones, *Eur. J. Org Chem.*, 2022, **2022**(34), e202101472.